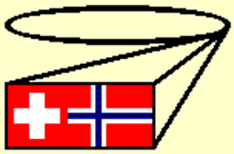

The Swiss-Norwegian Beam Lines at ESRF

03/04

ACTIVITY REPORT

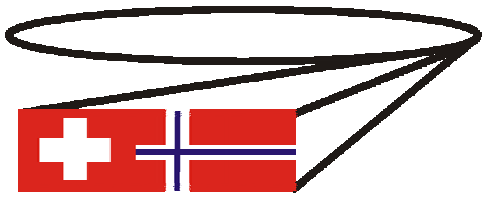

The Swiss-Norwegian Beamlines at ESRF

ACTIVITY REPORT 2003 - 2004

Contents ***Page***

This year the SNBL can look back on ten years of catering to the diverse needs of the Swiss, Norwegian and indeed ESRF general user communities. We do not have to blow our own trumpet – the Director of the ESRF has stressed the invaluable contribution made by SNBL to the scientific output of the facility as a whole.

Although we are working in uncertain times, I have confidence that under the steady stewardship of our new Director the SNBL will adapt to the changing requirements of the user community. Competition with other ESRF beamlines or indeed alternative synchrotron facilites is to the good – it sharpens us. A particularly apt example is the EXAFS upgrade which has a particular focus on greatly improving data quality and therefore will have the potential to attract especially those users with requirements for more sophisticated *in-situ* experiments. Certainly, the energy range offered is second to none.

I would like to pay tribute to the SNBL staff for their dedication in ensuring that the efficient running of the beamlines continues.

David G. Nicholson

Vice-Chairman SNBL

This report presents an overview of the SNBL's activity from January 2003 to December 2004. As usual, some experimental results have not yet been fully analyzed and published, and consequently the articles presented here give only a partial view of our activities. However, even a partial view is impressive.

The years 2003-2004 have been another productive period both for the SNBL team and for its user community. A number of technical developments have taken place during the year, including the commissioning of the new CCD detector on the KM6 diffractometer and the test-projects successfully using the combination of techniques (for example, X-ray diffraction + Raman). The other noteworthy changes during the last year include the commissioning of the multi-channel EXAFS detector, and an important rearrangement in the BM1B optics. The Swiss and Norwegian users exploited the high throughput of the beamlines with an increase in the publication rate. The number of papers which appeared in this period using data collected on SNBL reached an unprecedented level of 66 in publications 2003 and 71 in 2004.

An important milestone was passed in 2004, when SNBL was reviewed for the second time by an ESRF Committee (2–3 November). The Committee pointed out a number of outstanding publications both from the users and from the SNBL staff members. The Committee has concluded that the technical characteristics of the beamlines are sufficient in most places for the next 5 years. Following the recommendations of the Committee, the ESRF signed a renewal contract with SNBL for a further five years. Several of the suggestions and recommendations of the Committee are now being implemented on SNBL. For example, we have taken steps to improve the level of scientific collaborations between the SNBL project team and the home institutes of the user community, as well as to promote the contacts with national synchrotron facilities such as the Swiss Light Source. In addition, we are planning a closer collaboration between SNBL and the Dutch-Belgian beamline DUBBLE. This collaboration will include an exchange of beamtime, shared hardware (such as cryostats and furnaces), access to infrastructure (such as workshop facilities and chemistry laboratory) and R & D projects of mutual interest.

The beamline review process also provided the impetus to consider and to develop some of the scientific themes, which are likely to dominate the activities of SNBL in the coming years. There will be many technical developments needed at SNBL in order to keep pace with the demands and requirements of our scientific community. Some of these developments are addressed in the following status report for our two beamlines.

We hope that you enjoy reading the Highlights of 2003-2004 and we look forward to scientifically successful future for the Swiss-Norwegian Beam Lines.

V. DMITRIEV, P. PATTISON, H. EMERICH

SCIENTIFIC HIGHLIGHTS

STRUCTURES OF THE INTERMEDIATES IN THE MYOGLOBIN-PEROXIDE REACTION AND DI- AND TRI-NUCLEAR IRON CLUSTERS IN THE R2 SUBUNIT OF RIBONUCLEOTIDE REDUCTASE

Strand, K.R, H.P. Hersleth, Å.K. Røhr, B. Dalhus, S. Karlsen, M. Kolberg, K. Nilsson, Y. Hsiao, T.H. Rod, U. Ryde, C.H. Görbitz, and K. K. Andersson
(Oslo and Lund)

RIBONUCLEOTIDE REDUCTASE

The enzyme ribonucleotide reductase (RNR) catalyzes the reduction of the four ribonucleotides to the corresponding deoxyribonucleotides, which is essential for DNA synthesis and repair in all living cells. RNR from mouse belongs to class Ia that is found in eukaryotes and some bacteria and viruses. Class I RNRs are composed of two homodimeric protein subunits, termed R1 and R2. The RNR subunit R2 contains a dinuclear iron center, which in its diferrous forms spontaneously reacts with O_2 to form a μ-oxo bridged diferric cluster and a stable tyrosyl radical. We have solved the first crystal structures of R2 from mouse with its native dinuclear iron center, both under reducing and oxidizing conditions (Fig. 1).
The dinuclear iron center is located within a four-helix bundle and is coordinated by

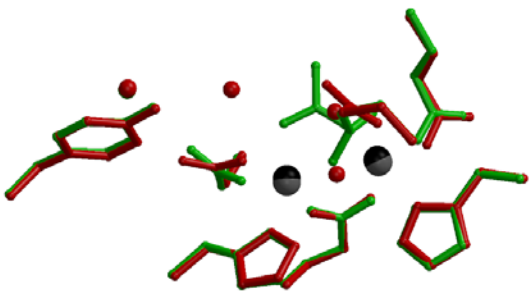

Fig. 1 Overlay of the reduced (green) and oxidized (red) structure of the dinuclear cluster of mouse R2 RNR [1].

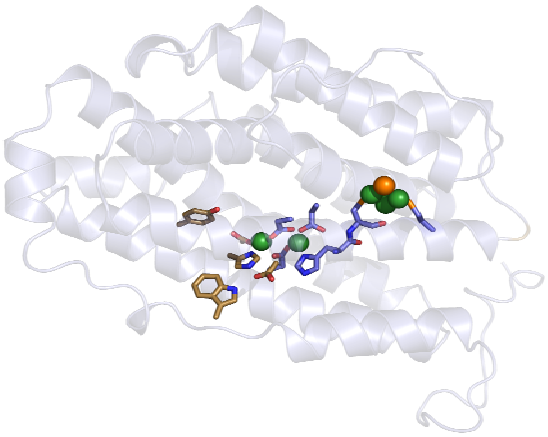

Fig. 2 Overview of the diiron cluster and a novel trinuclear metal cluster. The electron transport pathway is indicated in yellow.

carboxylate (Glu/Asp) and histidine side chains from the four helices (Fig 2).

Under reducing conditions, the bridging ligand Glu-267 of mouse R2 adopts the μ-(η^1,η^2) coordination mode, which is postulated to be very important for proper oxygen activation. The main difference upon oxidation is the introduction of the μ-oxo bridge and a large carboxylate shift of the flexible amino acid Glu-267. In addition, we have published several structures of the reduced form of mouse R2 obtained under different reducing conditions, very flexible arrangements of the carboxylate ligands of the diiron center are observed [2]. All the structures of mouse R2 confirm that the diiron center is connected with the surface via a relatively open hydrophobic channel. Two conserved phenylalanine residues in the hydrophobic environment around the diiron center are observed in opposing conformations in mouse R2 compared to *E. coli*. Together with the flexible carboxylate ligands, this novel conformation of the phenyl rings might contribute to the lower affinity and cooperative binding of iron in mouse R2 [1-4].
Several spectroscopic techniques have revealed hydrogen bonds to the phenoxyl oxygen of the tyrosyl radical in mouse R2. ENDOR measurements on the tyrosyl radical in mouse R2 confirmed that there

is an H/D exchangeable proton in mouse R2, and that it is located at a distance of 1.89 Å from the phenoxyl oxygen and in an angle slightly below the tyrosyl ring plane and pointing away from the phenoxyl oxygen. Since no crystal structure of the active radical form has been reported, we have proposed models for the movement of waters and/or tyrosyl radical site when non-radical mouse met-R2 is oxidized to the radical form based on our crystal structures, in agreement with the previous ENDOR study (Fig. 3) [2].

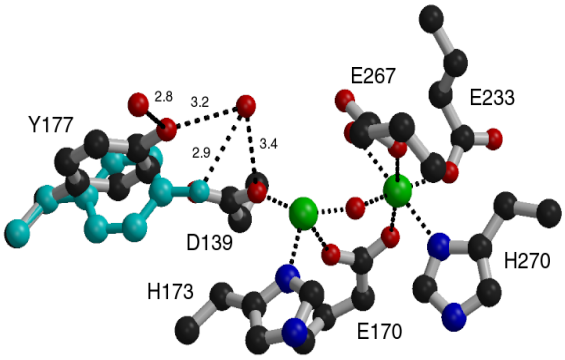

Fig. 3 Model of movement of radical.

In one structure about 10 Å away from the diiron-cluster, high peaks were observed in the initial Fo-Fc difference map. A trinuclear metal cluster was modeled into the peaks (Fig. 4). It is not clear yet if the trinuclear cluster has any biological relevance.

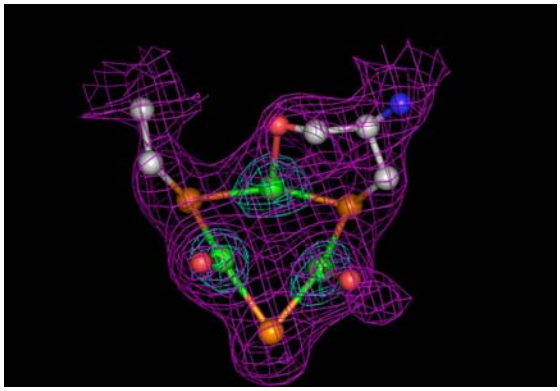

Fig. 4 The novel trinuclear metal cluster, where the electron density map (2Fo-Fc) is contoured at 1.5σ (magenta) and 10σ (cyan).

MYOGLOBIN

In haem-based peroxidases or oxygenases the ferryl [$Fe^{IV}O$] form is important in the compound I and compound II complexes, which are two and one oxidation equivalents higher than the ferric [Fe^{III}] form, respectively. The reaction cycle is shown in Scheme 1, and we have tried to trap the different intermediates of these reactions in myoglobin. To confirm or rule out reduction of the metal centre a light absorption spectrum of the crystal is needed after data collection. We have for the last two years regularly used the microspectrophotometer at SNBL for these studies.

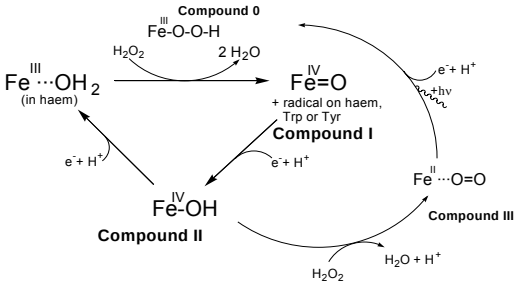

Scheme 1 Reaction scheme for the reaction between myoglobin and peroxides

High resolution structures of the myoglobin compound II have been solved at pH 5.2 [5], 6.8 and 8.7. Formation of the correct intermediate has been confirmed by single crystal light absorption spectroscopy (micro-spectrophotometry). For the compound II intermediate we do not observe any reduction due to radiation damage.

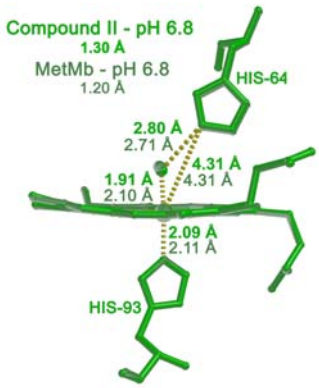

Fig. 5 Crystal structure of myoglobin compound II at pH 5.2 compared to resting myoglobin

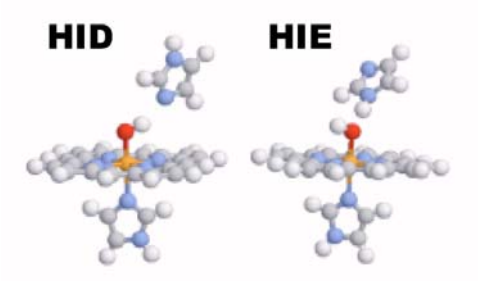

Fig. 6 Models with different protonation states of the histidine.

The crystal structure of compound II at pH 6.8 is shown in Fig. 5 together with the radiation influenced resting ferric (metMb) myoglobin. The most interesting point is the relatively long Fe–O bond of 1.9 Å. The structure at pH 5.2 has been further refined by quantum refinement to give a more detailed picture of the state [6]. In Fig. 6 two models with different protonation states of the distal histidine used in the quantum refinement are shown [6].

By using a higher peroxide concentration compound II can react further generating compound III (an oxy-complex). This intermediate was reduced by the synchrotron radiation as shown by microspectrophotmetry giving an equivalent of compound 0 (Fe^{III}-peroxide). The structure of this intermediate is shown in Fig. 7.

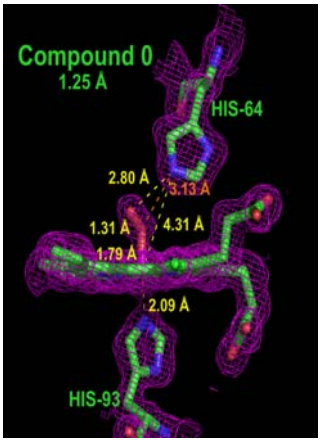

Fig. 7 Crystal structure of the myoglobin compound 0 equivalent

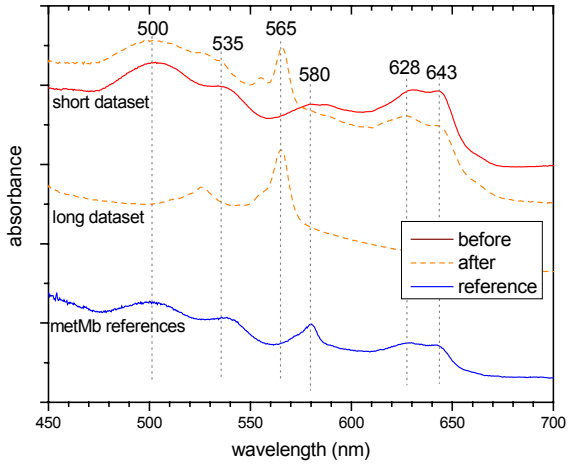

Fig. 8 Light absorption spectra of ferric myoglobin (metMb) crystals before and after data collection.

By using 1/20 of the exposure time for a normal myoglobin dataset (=short dataset), a mixture of the normal resting form and the radiation reduced form (peaks at 525 and 565 nm) were observed by micro-spectrophotometry as seen in Fig. 8. Further efforts will be made in the search of the unreduced ferric myoglobin structure.

References:

1. Strand, K.R. Ph. D. thesis Univ. of Oslo, 2004
2. Strand, K. R., Karlsen, S., Kolberg, M., Røhr, Å. K., Görbitz, C. H., and Andersson, K. K. (2004). *J. Biol. Chem.* **279**, 46794-46801
3. Strand, K. R., Karlsen, S., Andersson, K. K. (2002). *J. Biol. Chem.* **277**, 34229-34238
4. Strand, K. R., Yang, Y.-S., Andersson, K. K., and Solomon, E. I. (2003). *Biochemistry* **42,** 12223-12234
5. Hersleth, H.-P., Dalhus, B., Görbitz, C.H. and Andersson, K.K. (2002) *J. Biol. Inorg. Chem*. **7**, 299-304.
6. Nilsson, K., Hersleth, H.-P., Rod, T.H., Andersson. K.K. and Ryde, U. (2004) *Biophys. J*. **87**, 3437-3447

NEGATIVE THERMAL EXPANSION AND INTERMEDIATE VALENCE STATE IN Pr METAL

A. Kuznetsov, V. Dmitriev, O. Bandilet, H.-P. Weber (Grenoble, Lausanne)

The fundamental principles of thermodynamics are very logical and natural. Indeed, if one compresses a solid it is natural to expect it to reduce the volume; if a sample is heated the volume logically should increase. However, such logic is based on the independence of different microscopic degrees of freedom, while the solids with strong coupling between electrons show exciting effects sometimes violating the logic of the classical principles. The rare-earth metals and their compounds exemplify systems whose properties are governed by strongly correlated electrons. These latter make possible, against simple logic but in agreement with advanced principles, the lattice compression with the temperature increase.

Our x-ray diffraction study at high temperature showed that Pr metal undergoes a phase transition from dhcp to fcc in the temperature range 575-1035 K. An Invar-like behaviour of the lattice parameters was found for the high-temperature cubic phase and attributed to an interaction between normal thermal expansion and contraction induced by valence variation, the latter being observed for the first time in metallic Pr.

The first indication of the fcc phase appears in Pr at about 575 K, under equilibrium as well non-equilibrium conditions. The intensity of the fcc peaks increases with rising temperature, while the intensity of the dhcp peaks decreases continuously. The Debye-Scherrer diffraction patterns show a progressive recrystallization of the sample, even at low temperature: the initially homogeneous diffraction rings, belonging to the dhcp structure transform into spotty ones. The fcc diffraction patterns appear first as perfectly isotropic broadened rings [Fig. 1(a)] indicating initially random orientation of numerous nucleation centres. The fcc diffraction rings remain homogeneous over a considerable temperature range but decrease in width with increasing temperature, the effect corresponding to an increase in crystallite size.

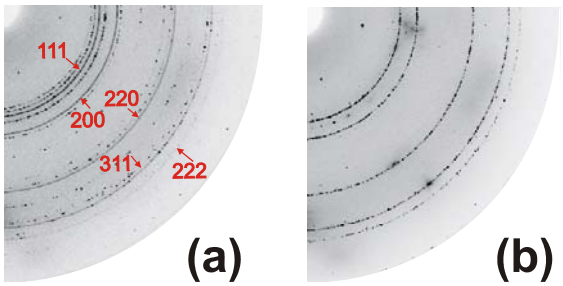

Fig. 1 Debye-Scherrer diffraction rings of Pr as recorded on an image plate. (a) T=840 K; fcc diffraction rings are indexed. (b) T=1055 K.

The properties of the cubic phase of Pr are very intriguing. The cubic structure has initially a negative thermal expansion coefficient. It then changes its sign but still keeps an anomalously low (almost zero) value over a wide temperature region and only starts exhibiting a normal temperature expansion from about 800 K upward. This behaviour can be seen clearly in the variation of the interlayer spacing, $d_{[111]c}$, which is compared, in Fig.2, with its hexagonal analogue $d_{[004]h}$ (both are d-spacings between hexagonal close-packed atomic planes). One can see a monotonic increase in the dhcp interlayer. In contrast with the dhcp structure, the fcc structure shows, first, a negative thermal expansion and then a stabilization of the lattice parameter.

The mechanism most consistent with our experimental observation relates to the valence transition reported for several rare-earth metals.

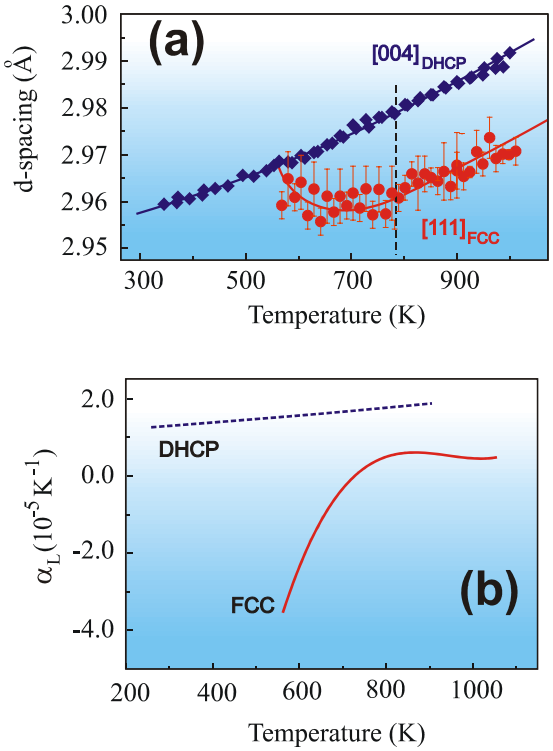

Fig. 2 Linear thermal expansion of Pr metal: (a) Blue diamonds correspond to the dhcp phase, red circles - to the fcc phase. (b) Smoothed linear expansion coefficients α^{dhcp} and α^{fcc}.

These metals are known to exhibit a valence variation with pressure and temperature. The valence variation between the low- and high-valence limits evidently should yield variation of the lattice constants in the sense that they attain values corresponding to $n+\Delta$ ($0<\Delta<1$), intermediate to those expected for pure n- and (n+1)-valence metal.

Experimental evidence for valence variation, i.e. the existence of intermediate valence states, were reported for at least three members of the rare-earth metal family: Ce, Eu, and Yb. In Ce a discontinuous variation of the valence was found to cause the observed isostructural γ(fcc)-α(fcc') transformation through the corresponding atomic volume collapse. In contrast, in Eu, the valence varied continuously over a wide pressure range including the bcc-hcp phase boundary, and no remarkable anomalies in the lattice parameter behaviour were observed. Both types of variation, continuous and discontinuous, can be treated within the framework of an unified phenomenological model of an isostructural phase transition. Such a Landau-type theoretical approach is known to deal with a single-component order parameter spanning the totally symmetrical (identity) irreducible representation of the parent phase space group. A scalar (isotropic) physical quantity, such as volume or valence deviation, perfectly fits this role.

The non-equilibrium energy (Landau potential) associated with the simplest model of an isostructural phase transition has the form:

$$F(\Delta)=a_1\Delta+a_2\Delta^2+\Delta^4.$$

This potential correspond to one of the elementary catastrophes, namely, the cusp catastrophe. Figure 3 shows a 3-d diagram of the equilibrium surface of the order parameter Δ. It is easy to predict the valence magnitude behaviour for the different paths, i.e. on the different plane sections of the equilibrium surface.

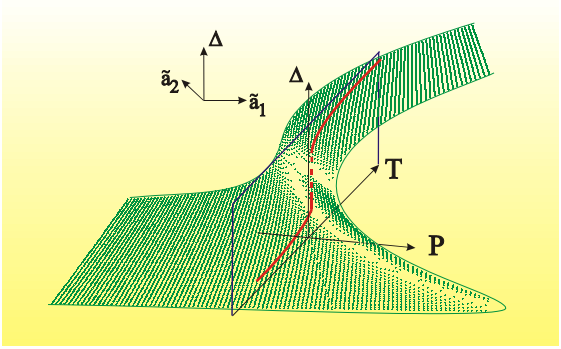

Fig. 3 Surface of valence variation.

Our experimental data on equilibrium thermal expansion can be recalculated into the valence temperature variation by using the alloy model. For this

purpose we can consider the elemental Pr crystal as a solid solution of fraction *x* of tetravalent and fraction (1-*x*) of trivalent metal. An average metallic radius of Pr atom, which determines inter-atomic distances and lattice parameters of such a "disordered alloy", is equal to $R=xR^{4+}+(1-x)R^{3+}$, where R^{3+}=1.83 Å corresponds to the trivalent $4f^3 5d^0 6s^2$ electron configuration and R^{4+}=1.658 Å corresponds to the tetravalent $4f^2 5d^1 6s^2$ one. In order to get the contractive part of the atom size variation, the difference $\Delta d=d_{[111]fcc}-d_{[004]dhcp}$ can be used [Fig.2(a)]. One can find the values for intermediate valence of Pr by taking into account that $x\equiv\Delta$ and using an equation identical to that for the atomic radius R, $\nu=4\Delta+3(1-\Delta)$.

Figure 4 shows the temperature variation of the valence in the fcc phase of Pr metal obtained as just described. The three curves represent sections of the equilibrium surface [Fig. 3] in the vicinity of the critical point.

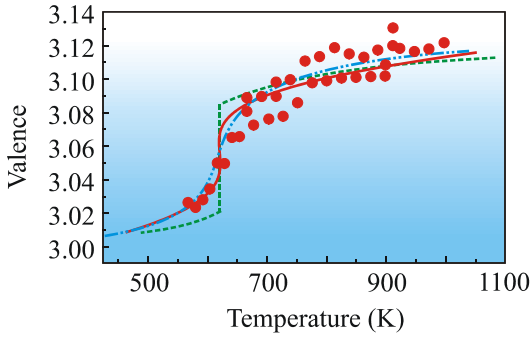

Fig. 4 Praseodymium valence variation in the fcc phase, data from three different experimental runs in isotropic heating conditions are used. Lines show the theoretically predicted valence behaviour for the path far from the critical point (dashed), at the critical point (solid), and beyond the critical point, (dashed-dotted).

One can see that the distributionof experimental points corresponds to a thermodynamic path passing very close to the critical point, in the domain of smooth variation of the order parameter.

A.Kuznetsov, V.Dmitriev, O.Bandilet, H.P.Weber, *Phys.Rev.B* (2003) **68**, 064109.

SPIN TRANSITION AS SEEN FROM DIFFRACTION EXPERIMENTS AND LANDAU THEORY

K. W. Törnroos, D. Chernyshov, M. Hostettler, B. Vangdal, and H.-B. Bürgi (Bergen, St.-Petersburg, Bern, Grenoble)

Some complexes of 3d metals change colour, magnetization and volume as a function of temperature, pressure, laser irradiation and magnetic field. The associated solid-state switching processes not only hold a potential for technological applications like memory or display devices, they are also of fundamental scientific interest.

For certain octahedral d^6 iron(II) complexes the switching is linked to a spin conversion between two states of nearly equal energies (low spin (LS) S=0, $t_{2g}^6e_g^0$; high spin (HS) S=2, $t_{2g}^4e_g^2$).

However, molecular bi-stability is only one of the factors governing the changes of physical properties in the solid, interactions between the ions and molecules in the crystal are another factor, one that may lead to multi-stability as well. Small multi-stable and switchable molecular arrays are of interest as elementary units for future technologies based on ternary and higher order logics.

In the spin crossover family only tri-stability has been found up to now, a scenario often called a “two step transition”. Inconclusive and contradictory characterizations of the nature of the intermediate phase (IP) have been given, most interpretations of the experimental information favouring a glass-like state with short-range correlations between HS and LS molecules.

We have investigated crystals of $[Fe^{II}(2\text{-pic})_3]Cl_2\cdot EtOH$ (2-pic: 2-picolylamine) by X-ray diffraction at 16 temperatures between 12 and 298 K using 2D detectors at the SNBL at ESRF. We found three-stable states, but the diffuse scattering expected from a glass-like IP was not observed. Instead additional Bragg reflections were found between T_1 ~124(1) K and T_2 ~114(1) K indicating two successive phase transitions of the order-disorder type. They disclose long-range correlations between LS and HS molecules, thus corroborating a superstructure in the IP (Fig. 1).

A Landau-type phenomenological analysis of the diffraction data leads to a generic phase diagram, which appears to apply to related spin crossover compounds as well. The model for bi-stability is based on the experimental observation that a collective spin switch may be described as an isostructural transition with a totally symmetric order parameter. The phase diagram with the minimal set of parameters corresponds to the well-known diagram for a cusp catastrophe and successfully maps the experimental observations (Fig. 2).

An extension of the model in which the spin transition is coupled with a structural transformation accounts for tristability, the long-range ordering of LS and HS complexes and for the coupling of structural and isostructural order parameters (see Fig.3 for the corresponding phase diagram).

A rich variety of spin transition scenarios has been observed serendipitously in a family of six chemically and structurally very closely related spin crossover compounds, namely the six solvates of $[Fe^{II}(2\text{-pic})_3]Cl_2$ with methanol, ethanol, 1-propanol, 2-propanol, t-butanol and allyl-alcohol. These compounds show: (1) very similar crystal structures at 200K, (2) different structural phase transitions upon changing temperature, and (3) different spin conversion behaviour (Fig. 3).

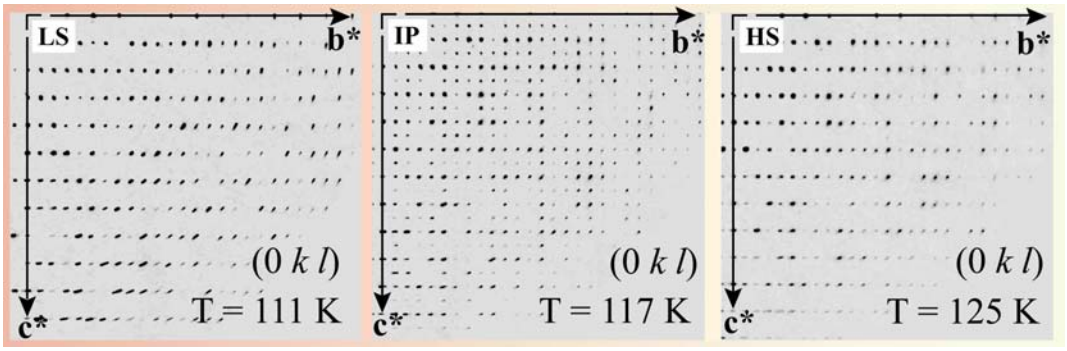

Fig. 1. Reconstructed reciprocal layers for the solvate $[Fe^{II}(2\text{-pic})_3]Cl_2$ ethanol. Additional Bragg reflections in the intermediate phase indicate ordering of spin states.

An extension of the model in which the spin transition is coupled with a structural transformation accounts for tristability, the long-range ordering of LS and HS complexes and for the coupling of structural and isostructural order parameters (see Fig.3 for the corresponding phase diagram). A rich variety of spin transition scenarios has been observed serendipitously in a family of six chemically and structurally very closely related spin crossover compounds, namely the six solvates of $[Fe^{II}(2\text{-pic})_3]Cl_2$ with methanol, ethanol, 1-propanol, 2-propanol, t-butanol and allyl-alcohol. These compounds show: (1) very similar crystal structures at 200K, (2) different structural phase transitions upon changing temperature, and (3) different spin conversion behaviour (Fig. 3).

We interpret this observation to mean that, in spite of their static similarity, the flexibility of the six crystal structures is quite different. The free energy surface of this structure type seems to exhibit several minima, which differ only slightly, but still sufficiently so to induce different behaviour for the six alcohol different solvates.

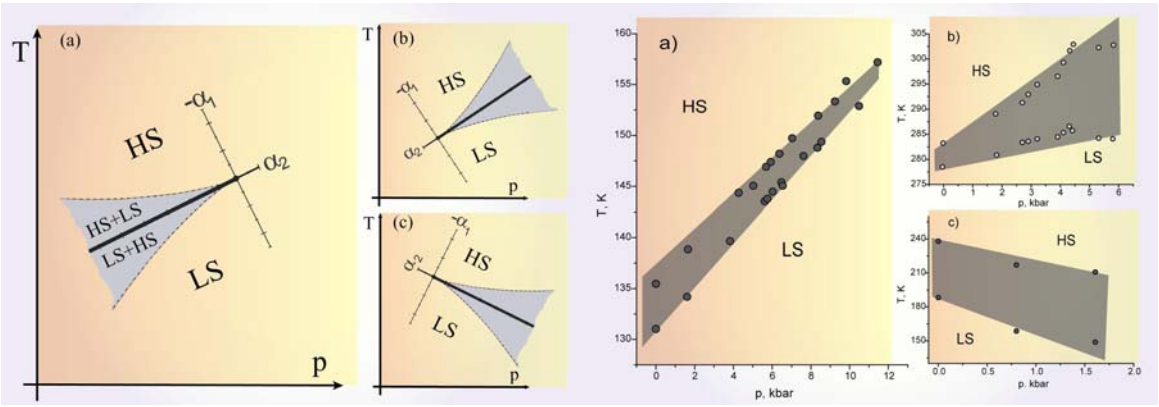

Fig. 2 *Left*: Theoretical phase diagrams for an isostructural spin transition. The grey area between the spinodal lines (dashed) marks the region of phase coexistence. The bold line delineates the first-order transition regime. The orientation of the phase diagram in the *p*-*T* plane depends on the temperature and pressure evolution of the phenomenological coefficients.
Right: Experimental observations of hysteresis widths as a function of pressure and temperature for different spin crossover compounds. The grey zones emphasize the convergence of the domain of phase coexistence towards the critical point.

A rich variety of spin transition scenarios has been observed serendipitously in a family of six chemically and structurally very closely related spin crossover compounds, namely the six solvates of $[Fe^{II}(2\text{-pic})_3]Cl_2$ with methanol, ethanol, 1-propanol, 2-propanol, t-butanol and allyl-alcohol. These compounds show: (1) very similar crystal structures at 200K, (2) different structural phase transitions upon changing temperature, and (3) different spin conversion behaviour (Fig. 3).

We interpret this observation to mean that, in spite of their static similarity, the flexibility of the six crystal structures is quite different. The free energy surface of this structure type seems to exhibit several minima, which differ only slightly, but still sufficiently so to induce different behaviour for the six alcohol different solvates.
These findings together with the detailed structural information collected with the help of synchrotron radiation, illustrate that cooperative transitions between two states in crystals built from bi-stable constituents are but the simplest among a multitude of possible scenarios of spin crossover only some of which have been observed experimentally so far.

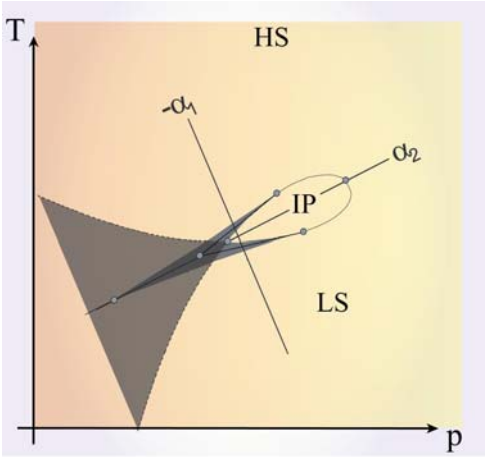

Fig. 3 Generic phase diagram for a two-step transition.

Principal publications:

M. Hostettler, K. W. Törnroos, D. Chernyshov, B. Vangdal & H. B. Bürgi. *Challenges in Engineering Spin Crossover: Structures and Magnetic Properties of Six Alcohol Solvates of Iron(II) Tris(2-picolylamine) Dichloride* ANGEWANDTE CHEMIE INT. ED. **43** (2004) 4589.

D. Chernyshov, H.-B. Bürgi, M. Hostettler & K. W. Törnroos *Landau theory for spin transition and ordering phenomena in Fe(II) compounds* PHYSICAL REVIEW B **70** (2004) 094116.

D. Chernyshov, H.-B. Bürgi, M. Hostettler & K. W. Törnroos *Insights into a Spin Transition: Three Stable States of a Spin-crossover Crystal Built from Bi-stable Molecules*, ESRF HIGHLIGHTS, **44** (2003)

D. Chernyshov, M. Hostettler, K. W. Törnroos & H.-B. Bürgi *Ordering phenomena and phase transitions in a spin crossover compound* ANGEWANDTE CHEMIE INT. ED. **42** (2003) 3825-3830.

HIGH-RESOLUTION POWDER DIFFRACTION, AN IRREPLACEABLE TOOL FOR COMPLEX STRUCTURES OF INTERMETALLIC COMPOUNDS AND HYDRIDES

Radovan Černý, Guillaume Renaudin and Klaus Yvon
(Genéve, Clermont-Ferrand)

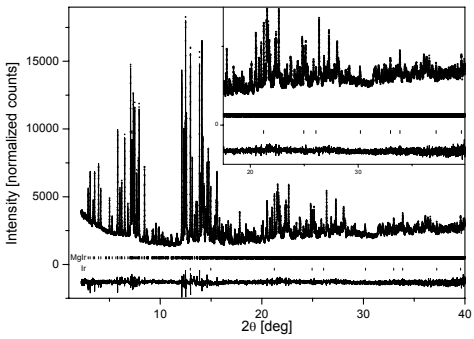

Fig. 1 Rietveld plot of MgIr (R_{wp} = 0.094, χ^2 = 3.02). Observed (dots) and calculated (solid line) synchrotron (SNBL) powder diffraction patterns (λ = 0.50012 Å) are shown with difference curve below. Ticks indicate the line positions of the main phase MgIr (R_B = 0.056) and the impurity phase Ir.

The high-resolution powder diffraction, especially using synchrotron radiation, has become an irreplaceable tool in the characterization of new intermetallic compounds and metal hydrides. In the past 3 years we have solved and characterized around 20 new compounds using the high-resolution powder diffractometer of the SNBL. The examples presented here show a complexity of the crystal structure fully characterized (MgIr) and a tiny monoclinic distortion revealed ($LaMg_2NiD_7$) when high-resolution data are available.

The crystal structure of MgIr was solved and refined using the synchrotron powder diffraction data measured at the wavelength of λ=0.50012 Å (Fig. 1). High-energy X-rays were chosen here to maximize diffracted intensities from this highly absorbing compound. The data were indexed with the orthorhombic cell *a* = 18.46948(6) Å, *b* = 16.17450(5) Å, *c* = 16.82131(5) Å, and the space group *Cmca* identified from the observed extinction conditions. The structure was solved by the global optimization of a structural model in direct space using the recently developed program Fox [1]. For more details on the optimal structure solution procedure see [2]. The global optimization method was successfully applied here to a 25-atoms structure with the close-packing and high symmetry. Alternative methods using integrated intensities extracted from the powder pattern (direct methods or Patterson synthesis) have failed, probably because of difficult recognition of a structural motif the methods using extracted integrated intensities from the powder pattern (direct methods or Patterson synthesis) have failed, probably because of difficult recognition of a structural motif either in E- or in Patterson maps.

$LaMg_2NiH_7$ is an interesting compound from both fundamental and technological points of view. The particularity of this hydride is the way of synthesis: the intermetallic compound $LaMg_2Ni$ absorbs hydrogen near ambient conditions forming the non-metallic hydride $LaMg_2NiH_7$ which has a nearly unchanged metal host substructure (atom shifts < 0.7 Å) [3]. The transition is induced by a charge transfer of conduction electrons into tetrahedral $[NiH_4]^{4-}$ complexes having closed-shell electron configuration [4]. $LaMg_2Ni$ is the first ternary compound known to absorb hydrogen without important rearrangement of the metal host substructure that leads to a metal-semiconductor transition. A complete structural characterisation of the hydride was of primary importance to elucidate the metal - semiconductor

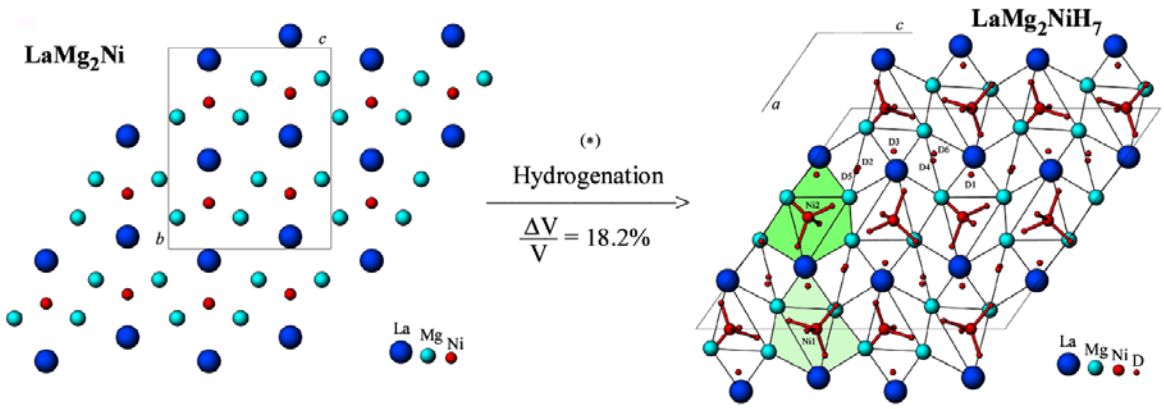

Fig. 2 Structure representation of orthorhombic intermetallic compound $LaMg_2Ni$ (left) and monoclinic hydride $LaMg_2NiD_7$ (right).

transition. Figure 2 shows the crystal structures, before ($LaMg_2Ni$) and after ($LaMg_2NiH_7$) hydrogenation. The structure of monoclinic $LaMg_2NiH_7$ ($LaMg_2NiD_7$) was solved and refined by using synchrotron and neutron powder diffraction ($P2_1/c$, a = 14.0164(6) Å, b = 4.7146(2) Å, c = 16.0572(8) Å, β = 125.222(2)°, Z = 8). Synchrotron powder diffraction data (λ=0.499490 Å) was useful to elucidate the true symmetry and position of the metal atoms (8 sites), whereas neutron powder diffraction data (D2B at ILL, Grenoble, λ= 1.594 Å) was useful to locate deuterium atoms (14 sites).

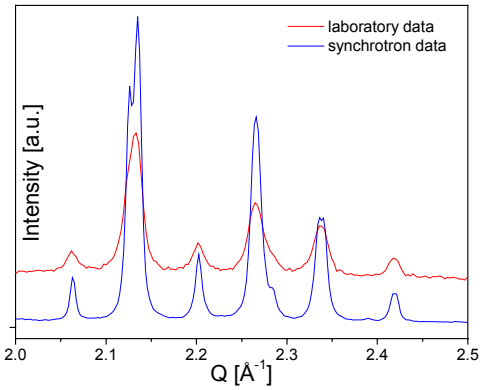

Fig. 3 Selected part of powder diffraction patterns of $LaMg_2NiD_7$: laboratory data (Cu $K\alpha_1$, red) and synchrotron data (λ=0.499490 Å, blue). Only the synchrotron data show the peak splitting due to the monoclinic distortion.

Only the high-resolution synchrotron data (Figure 3) allowed us to observe a tiny monoclinic distortion and a doubling of the cell volume of the $LaMg_2NiH_7$ lattice that was previously indexed using the laboratory data in an orthorhombic cell corresponding to the expanded cell of the intermetallic compound $LaMg_2Ni$. Only the true monoclinic symmetry allowed us to identify the well-ordered hydrogen (deuterium) network.

References

[1] Favre-Nicolin V. and Černý R.: *J. Appl. Cryst.*, **35** (2002) 734
[2] Černý R., Renaudin G., Favre-Nicolin V., Hlukhyy V. and Pöttgen R.: *Acta Cryst.* **B60** (2004) 272-281
[3] Renaudin G., Guénée L. and Yvon K.: *J. Alloys and Compounds*, **350** (2003) 145-150
[4] Yvon K., Renaudin G., Wei C.M. and Chou M.Y.: *Phys. Rev. Let.*, **94** (2005) 066403

IN SITU SR-XRD STUDIES OF HYDROGEN ABSORPTION-DESORPTION IN $LaNi_{4.7}Sn_{0.3}$

Marit Stange, Jan Petter Maehlen, Volodymyr Yartys, Poul Norby, Wouter van Beek and Hermann Emerich
(Kjeller, Oslo, Grenoble)

$LaNi_5$-related hydrides have a wide range of applications including hydrogen storage and compression, H_2 purification and separation, heat management and nickel-metal hydride batteries. The convenient properties of $LaNi_5$ include: a desorption pressure slightly exceeding 1 bar at room temperature, considerably fast absorption and desorption kinetics and easy activation.
A problem with pure $LaNi_5$, however, is that after cycling its hydrogen absorption-desorption properties are partially deteriorated which goes in parallel with loss of crystallinity evidenced by a significant line broadening. After further cycling of the material, additional problems with disproportionation and reduced storage capacity appear.

Doping of $LaNi_5$ by different elements can dramatically improve cycle life of the alloys and reduce the problem with hysteresis, peak broadening and intrinsic degradation. One successful example is $LaNi_{4.7}Sn_{0.3}$ where element Ni is substituted by Sn. $LaNi_{4.7}Sn_{0.3}$ is very attractive for the negative electrode in Ni–MH batteries. A lowering of the plateau pressure and a decrease in hydrogen capacity is observed with increasing Sn content. It is also important to note that small Sn levels ensure a single-step formation and decomposition of the β - hydride preventing the formation of a destructive intermediate $LaNi_5H_{\sim 3}$ (γ-phase).

Structural phase transformations during hydride formation and decomposition in the advanced hydrogen storage alloy $LaNi_{4.7}Sn_{0.3}$, are studied by *in situ* synchrotron X-ray powder diffraction (SR-XRD). Temperature cycling between RT and 100 °C at H_2 pressures of 2–3 bar applied to $LaNi_{4.70}Sn_{0.30}H_{\sim 6}$ resulted in a reversible hydrogen absorption–desorption process. In addition, *ex situ* diffraction data of original and hydrogen cycled alloy, with focus on studies of the line-broadening phenomenon, are described.

Synthesis of the $LaNi_{4.7}Sn_{0.3}$-based β-hydride was achieved by applying the following procedure: The pre-activated $LaNi_{4.7}Sn_{0.3}$ was heated under vacuum to 200 °C before switching to hydrogen atmosphere (pH_2 ~2.6 bar) and cooling in H_2 to 25 °C. Refinement of the unit-cell dimensions of the collected in situ data showed that $LaNi_{4.7}Sn_{0.3}H_x$ reached a complete saturation with hydrogen. This conclusion is reached on the basis of comparison of the unit cell parameters from the Rietveld refinements [a = 5.3944(1) Å, c = 4.2813(2) Å, V = 107.89(1) $Å^3$ and the reference data for $LaNi_{4.75}Sn_{0.25}H_{6.1}$; a = 5.41 Å, c = 4.29 Å and V = 108.5 $Å^3$. The observed H-induced volume increase, $\Delta V/V$, is 21.1% both for $LaNi_{4.75}Sn_{0.25}$ and $LaNi_{4.70}Sn_{0.30}$. Hydrogen content $H/LaNi_{4.7}Sn_{0.3}$ estimated from comparison of the measured volume effects and literature data, is close to 6 atomic Hydrogens per formula unit (6 at.H/f.u.)

The hydride sample was cycled between 20 and 100 °C in H_2 gas. The cycling resulted in $\beta \leftrightarrow \alpha$ transformations during hydrogen release from $LaNi_{4.70}Sn_{0.30}H_{\sim 6}$ and loading of the α-phase by H_2. Fig. 1 shows the development of the powder

diffraction profiles during hydrogen desorption and absorption. At the applied pressure of 2.6 bar H_2, the β-phase decomposes in the T-range ~82.5–92.5 °C and forms back from α-phase between 70–80 °C. This difference is caused by application of not completely equilibrium conditions of the experiment; such type of conditions is anticipated during hydrogen loading/unloading in a MH hydrogen storage unit.

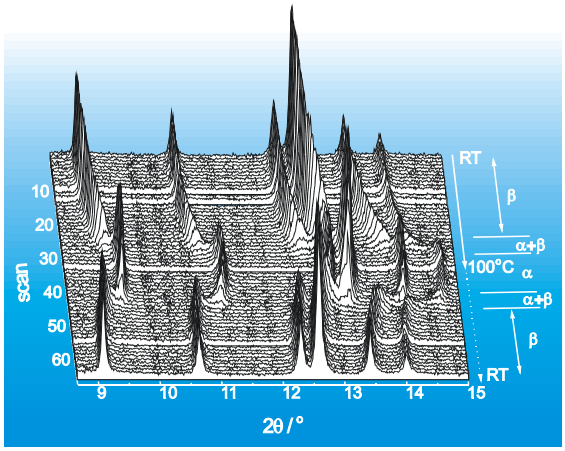

Fig. 1 Powder diffraction profiles during transformation of β-phase to α-phase on heating the saturated with hydrogen sample from 25 °C to 100 °C in H_2 gas and subsequent cooling to 25 °C to form back the β-phase.

Complete reversibility of the transformations was achieved on cycling. Unit-cell dimensions in the single-phase regions as determined by Rietveld refinements are shown in Fig. 2. The β-phase appears to have a large homogeneity range, most evidently seen from the variation along c ($\Delta c/c = -2.5$ %; $\Delta a/a = -1.2$ %; $\Delta V/V = -5.0$ % between 20 and 82.5 °C). A small hysteresis in the unit-cell dimensions takes place between hydrogen absorption and desorption which again is more pronounced along c [0.09 % along a vs 0.28 % along c at 60 °C]. Both solubility range and hysteresis of the α-phase are significantly smaller than for β. The change in unit cell dimensions is slightly more pronounced along a ($\Delta a/a = -0.12$ %; $\Delta c/c = -0.06$ %; $\Delta V/V = -0.30$ %). The homogeneity range of α is larger on absorption than during desorption while that of β is smaller.

The thermal expansion of $LaNi_{4.7}Sn_{0.3}$ during heating in vacuum over the same temperature range, 20–100 °C, was measured as a reference. This measurement yielded the values $\Delta c/c = 0.3$ %; $\Delta a/a = 0.4$ %; $\Delta V/V = 1.0$ % and led to the conclusion that the effects caused by changes in hydrogen solubility dominate the behaviour of the material and that the contribution from the thermal expansion/contraction effect is significantly weaker.

By disregarding the temperature dependent unit-cell changes in the rather narrow temperature window, the reduction in unit cell-volume of β corresponds to a homogeneity range of approximately $LaNi_{4.70}Sn_{0.30}H_{\sim 6.1-4.6}$ between 20 and 82.5 °C. The homogeneity range of α around 100 °C in H_2-atmosphere is very small judging from the small changes in unit-cell dimensions.

Complex transformations take place in the material in the area between the single-phase regions of the diagram. An α + β model with constant unit cell dimensions over the multiphase region, was considered as oversimplified as it did not provide satisfactory description of the data collected. Because of that, the unit-cell dimensions in the multiphase regions are not included in Fig. 2. The appearance of an intermediate hydride related to $LaNi_5H_3$ was considered and ruled out since none of the phases had unit-cell dimensions (c/a ratios) matching that of $LaNi_5H_3$ (c/a = 0.7669). This agrees

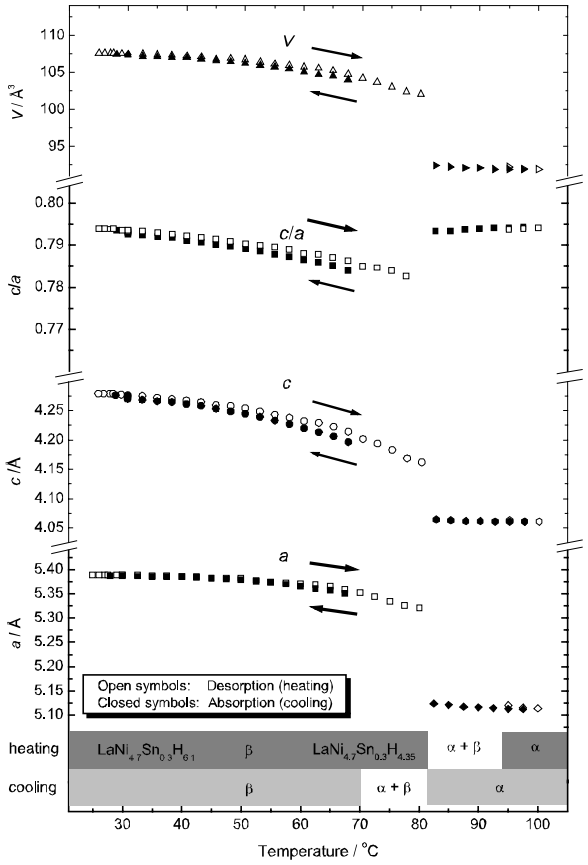

Fig. 2 Variations of the unit-cell dimensions of β-hydride and α-phase as a function of temperature

with the reference data for the related Sn substituted $LaNi_5$-based hydrides where an intermediate hydride was not observed and so far regarded as one of the most important reasons for the increased cycling stability of $LaNi_{5-x}Sn_xH_y$ compared to $LaNi_5$.

The experimental observations of this work allow a suggestion that the time resolution of the data is not sufficiently high to explain the area of phase transformations. Further studies with a time interval of 3–5 sec for each collected data set allowing to resolve the problem, are planned. A variation of the unit-cell dimensions over the two-phase region and a formation of new phases could be extra factors, which should be considered to explain the transformations. A possible inhomogenous distribution of hydrogen in the sample is also possible.

Finally, to study the effect of hydrogen cycling on the line widths of $LaNi_{4.70}Sn_{0.30}$, experimental half widths of selected reflections (conventional PXD data; Cu $K\alpha_1$; FWHM normalized with selected Si-reflections) of $LaNi_{4.70}Sn_{0.30}$ (annealed at 950 °C) were compared to those of the pre-cycled sample (exposed to 5 cycles in hydrogen). The line broadening is most likely related to the creation of lattice defects and microstrain or partially caused by a non-complete release of hydrogen during cycling at RT. A significant broadening of the diffraction peaks (approximately doubling of the FWHM for the (110) reflection) is observed after cycling. This observation does not agree with the conclusion of claiming that upon substitution of Ni by Sn in $LaNi_{5-x}Sn_x$ this effect vanishes for $x \geq 0.20$.

The results can be summarized as follows:

(i) The β-hydride has a large homogeneity range from 4.6 to 6.1 at.H/f.u. $LaNi_{4.7}Sn_{0.3}$;
(ii) A small hysteresis effect takes place between hydrogen absorption and desorption.
(iii) The region of phase-structural transformations $\alpha \leftrightarrow \beta$ is very complex and a high time-resolution of the *in situ* studies is required to uncover its mechanism.

Journal of Alloys and Compounds (*Accepted for publication*).

EX SITU AND *IN SITU* CHARACTERIZATION OF HETEROGENEOUS CATALYSTS

J.-D. Grunwaldt, S. Hannemann, M. Ramin, M. Rohr, A. Baiker
(Department of Chemistry and Applied Biosciences, ETH Zürich)

Ex situ characterization of heterogeneous catalysts used for carbon dioxide fixation

The simultaneous use of carbon dioxide in chemical synthesis both as C_1-synthesis block and as solvent is an interesting strategy in green chemistry. However, the activation of the relatively inert carbon dioxide molecule requires the design of suitable catalysts. Using both homogeneous and heterogeneous catalysts for this purpose we have applied the above strategy in the formylation of amines using carbon dioxide and hydrogen as well as in the formation of propylene carbonate from propylene oxide and carbon dioxide.

XANES and EXAFS were used to identify the structure of both homogeneous and heterogeneous catalysts [1-3]. Figure 1 compares the Fourier transformed XANES spectra of the liquid solution of different ruthenium-based catalysts that were used in hydroformylation of methoxy propylamine: During the reaction $RuCl_2(dppe)_2$ was more active than $RuCl_2(PPh_3)_3$. XAS studies unravelled that the structure significantly changed under reaction conditions particularly for the first complex (probably formation of a hydride). Interestingly solid Ru/Al_2O_3 in the presence of dppe was a suitable catalyst system as well. As XANES (Fig. 1) and EXAFS data show, a similar homogeneous catalyst formed under reaction conditions as from $RuCl_2(dppe)_2$ [1]. Due to the high activity of $RuCl_2(dppe)_2$, we immobilized this complex on a silica matrix by different methods. Once again, structural characterization by EXAFS and XANES is used for catalyst characterization.

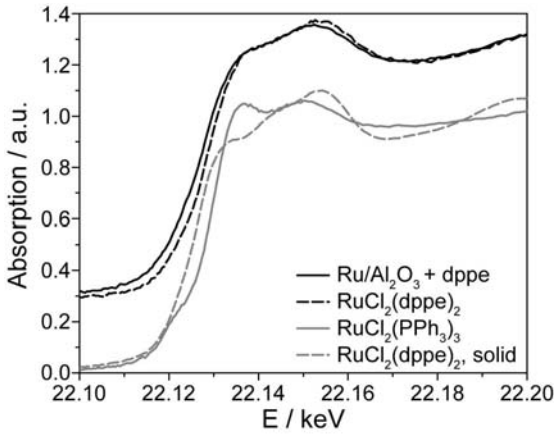

Fig. 1 Comparison of the Ru K-edge XANES spectra of the liquid solutions of Ru/Al_2O_3 + 1,2-bis(diphenylphospino)ethane (dppe), $RuCl_2(dppe)_2$ and $RuCl_2(PPh_3)_3$ after the hydroformylation reaction of carbon dioxide and hydrogen with methoxypropylamine (for details, cf. refs. [1,2]).

Zn-complexes with pyridine ligands in the presence of bromide are active catalysts for the cycloaddition of carbon dioxide to propylene oxide [3]. Similarly to the previous study, the prepared homogeneous and heterogeneous catalysts were

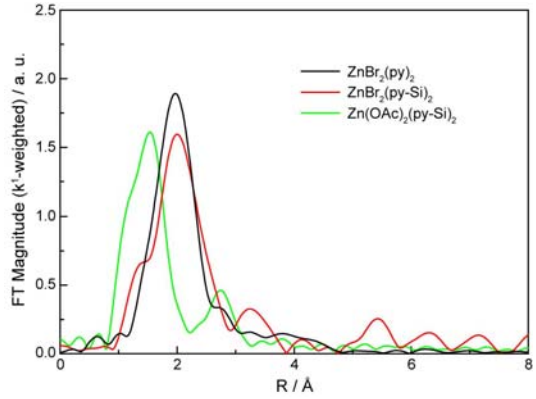

Fig. 2 Fourier transformed Zn K-edge EXAFS spectra of $Zn(py)_2Br_2$, and the on SiO_2 immobilized $Zn(py)_2(OAc)_2$ and $Zn(py)_2Br_2$-complexes (py-SiO_2, covalent linkage via ligand) showing the successful immobilization of the $Zn(py)_2Br_2$-complex, details in ref. [3].

analysed by EXAFS and XANES and uncovered that the Zn-complexes could be successfully immobilised on the silica matrix [3]. Figure 2 shows the spectra of a homogeneous $Zn(Py)_2Br_2$ complex, and the SiO_2 grafted complexes of $Zn(Py)_2Br_2$ and $Zn(Py)_2(OAc)_2$ (covalent linkage via the ligand). The similarity of the EXAFS spectra of $Zn(Py)_2Br_2$ and the immobilized counterpart indicates the successful preparation of the immobilized catalyst, further supported by EXAFS analysis.

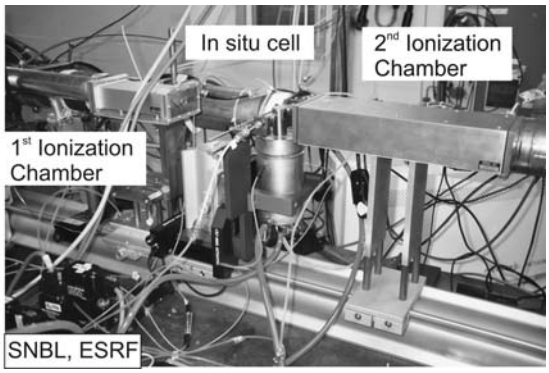

Fig. 3 *In situ* transmission EXAFS experiment for combined structural analysis and on-line catalytic studies of heterogeneous catalysts

Towards in situ XANES/EXAFS characterization of heterogeneous catalysts at SNBL

Figure 3 shows one of the setups adapted to the Swiss-Norwegian beamline to perform *in situ* experiments on heterogeneous catalysts during reduction in $5\%H_2/He$ but also under reaction conditions. In a systematic study, the suitability of different *in situ* cells were compared, that use either a catalyst pellet (pressed wafer) or powdered material [4]. Figure 4 compares for example the reduction of CuO/ZnO in the form of a pellet and as powder in a reaction cell. Striking differences were observed in the reduction behaviour that can be traced back to mass transport limitations in the pressed wafer.

CuO/ZnO-based catalysts are widely used in methanol synthesis and methanol reforming. The comparison of the reduction of differently prepared

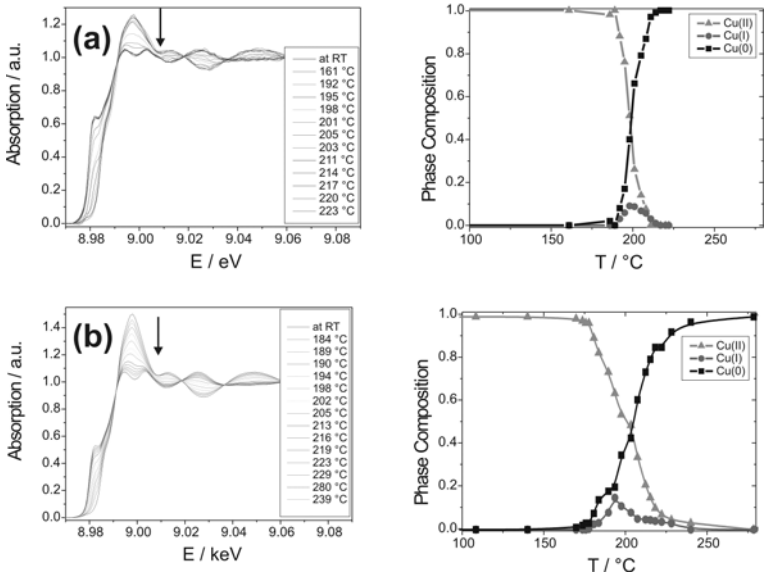

Fig. 4 Reduction of 30wt%CuO/ZnO in $5\%H_2/He$ using (a) an *in situ* cell with catalyst powder and (b) an *in situ* cell with a catalyst pellet; ramp rate 1°C/min, the arrow indicates the course of reaction, the phase composition was determined from linear combination analysis using reference spectra (cf. ref. [4]).

CuO/ZnO catalysts uncovered a variation of the reduction temperature of copper in the different catalysts. Furthermore, we found a direct relation between the onset temperature of the copper reduction and its activity in methanol synthesis [5]. To explore this relationship in more detail, catalyst characterization was combined with high throughput screening techniques, a project performed together with F. Schüth and C. Kiener at the Max-Planck Institute in Mülheim [6].

In situ characterization of heterogeneous catalysts combined with on-line gas analysis

The same setups were also used to uncover the oxidation state of Pd in PdO/ZrO_2 catalysts during low-temperature methane combustion. Both on-line catalytic results and the structure of PdO/ZrO_2-catalyst were obtained at the same time as depicted in Figure 5. The example shows a pre-reduced Pd/ZrO_2 catalyst that was more active in low temperature methane oxidation than a fully oxidized PdO/ZrO_2 catalyst. Obviously, the pre-reduced catalyst is re-oxidized upon heating in the reaction mixture to 500 °C. However, more careful analysis uncovered that the catalyst was not completely re-oxidized during this step which is probably the reason that it was more active than a completely oxidized PdO/ZrO_2 catalyst [7]. Hence, this indicates that metallic Pd species have a beneficial influence on the low temperature activity over PdO_x/ZrO_2 catalysts.

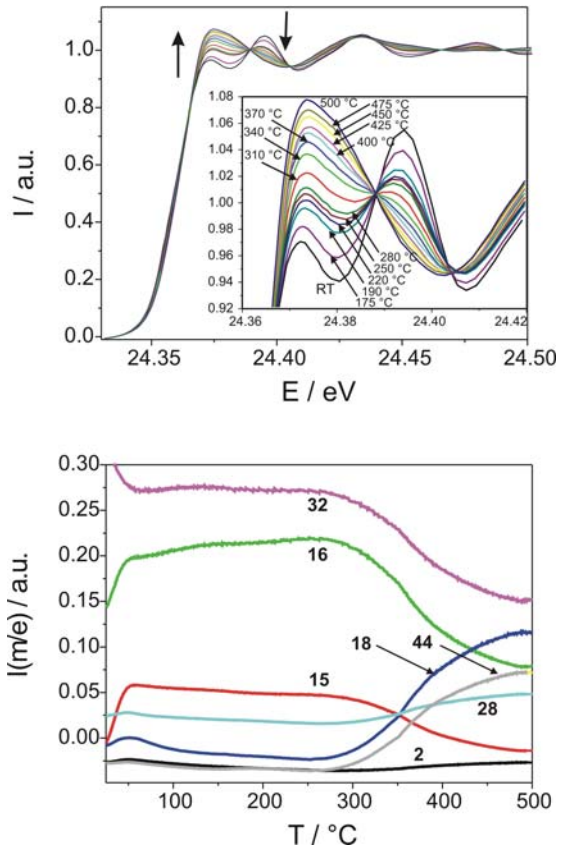

Fig. 5 Change in the XAS spectra at the Pd K-edge during heating a pre-reduced 30%Pd/ZrO_2 catalyst in 1%CH_4-4%O_2/He (top) combined with on-line gas analysis using a mass spectrometer (bottom), taken from ref. 7.

In conclusion, the *ex situ* and *in situ* XAS studies have considerably advanced our knowledge concerning the mentioned catalytic systems and criteria have been developed which allow to assess possible mass transfer influences in *in situ* experiments. In addition, new insight into structure-activity relationships of heterogeneous catalysts could be gained, where both the structure by XANES/EXAFS and the catalytic activity by on-line gas analysis could be determined.

Publications

[1] M. Rohr, J.-D. Grunwaldt and A. Baiker *Formylation with supercritical carbon dioxide over Ru/Al2O3 modified by phosphines: Heterogeneous or homogeneous catalysis?*
J. CATAL. **229** (2005) 149.

[2] M. Rohr, J.-D. Grunwaldt and A. Baiker *A simple route to highly active ruthenium catalysts for formylation reactions with hydrogen and carbon dioxide*
J. MOL. CATAL. A **226** (2005) 253.

[3] M. Ramin, J.-D. Grunwaldt and A. Baiker *Behavior of Homogeneous and Immobilized Zinc-based Catalysts in Cycloaddition of Carbon Dioxide to Propylene Oxide*
J. CATAL. (submitted).

[4] J.-D. Grunwaldt, M. Caravati, S. Hannemann and A. Baiker *X-ray Absorption Spectroscopy under Reaction Conditions - Opportunities and Limitations of in situ Monitoring and Time-Resolved Studies of Heterogeneous Catalysts*
PHYS. CHEM. CHEM. PHYS. **6** (2004) 3037.

[5] C. Kiener, M. Kurtz, H. Wilmer, C. Hoffmann, H.-W. Schmidt, J.-D. Grunwaldt, M. Muhler and F. Schüth *High-throughput screening under demanding conditions: Cu/ZnO catalysts in high pressure methanol synthesis as an example*
J. CATAL. **216** (2003) 110.

[6] J.-D. Grunwaldt, C. Kiener, F. Schüth and A. Baiker *X-ray Absorption Spectroscopy on Cu/ZnO Catalysts Selected by High-Throughput Experimentation Techniques*
PHYSICA T**115** (2005) 819.

[7] J.-D. Grunwaldt, M. Maciejewski and A. Baiker *In situ X-ray absorption study during methane combustion over Pd/ZrO_2 catalysts*
PHYS. CHEM. CHEM. PHYS. **5** (2003) 1481.

NEW TECHNIQUES AND METHODOLOGY

CHARACTERIZATION OF PROTEIN CRYSTALS GROWN IN A MAGNETIC FIELD

Some experiments have indicated that protein crystals grow more homogeneously and with lower mosaicity inside a high magnetic field than under normal crystallization conditions. It is also possible to levitate a protein solution due to its diamagnetism, thus simulating the conditions of weightlessness. Several attempts have been made to produce better quality crystals using these techniques, and now the appropriate methodology must be developed in order to characterize properly the quality of these crystals. This task is made complicated by the fact that the measurements must be made at room temperature, since flash freezing of protein crystals inevitably causes a deterioration in crystal quality. However, measurements at room temperature can easily lead to radiation damage, which in turn will falsify the results. We must first orient the crystal on a diffractometer, and then measure the rocking curves in a sufficient number of orientations to determine the angular dependence of the crystal mosaicity. It is essential that the crystal quality is determined in several orientations of the crystal, since experience has shown that crystals may show excellent reflection profiles in some direction and broad rocking curves in other orientations. All of these measurements must be carried out at room temperature and with the minimum exposure of the crystals to damaging X-rays.

In order to test the orientational dependence of crystal mosaicity, we need:

- An area detector for rapid determination of the orientation matrix
- Transfer of this information to a multi-axis diffractometer equipped with a point detector
- Measurement with high angular resolution of some selected reflections
- Fast throughput for systematic studies

The KM6 diffractometer on SNBL is ideal for this type of experiment. The CCD area detector and a point detector are simultaneously available on the same instrument. This instrument therefore combines the speed needed for rapid orientation of the sample, together with high angular resolution for the characterization of crystal quality. In an experiment proposed and carried out by D. Luebbert, A. Meents and E. Weckert (Hasylab) using public beamtime on BM1A, data were collected on hen egg-white lysozyme, thaumatin and trypsin. In studies of this type, a systematic approach is vital since individual crystals will not necessarily be representative of the bulk. In total it was possible for the team from Hasylab to characterize over 50 crystals in 3 days of beamtime.

In Fig. 1, we show the diffraction pattern of a crystal of hen egg-white lysozyme measured with the CCD detector on the KM6 diffractometer. In a data collection run lasting about 15 minutes, it was possible to determine the crystal orientation matrix with sufficient accuracy to allow individual reflection to be located with the point detector. Measurements of the rocking curves of equivalent reflections in this

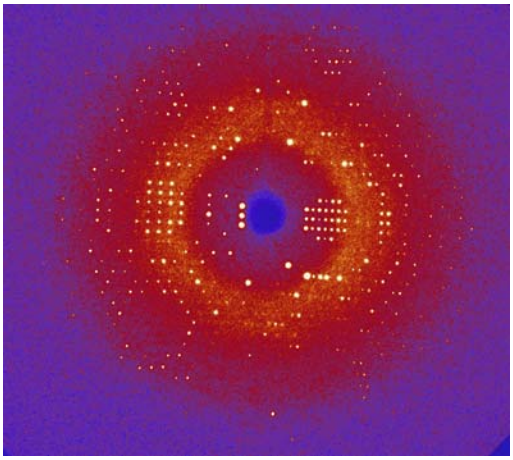

Fig. 1 CCD data for hen egg-white lysozyme at room temperature.

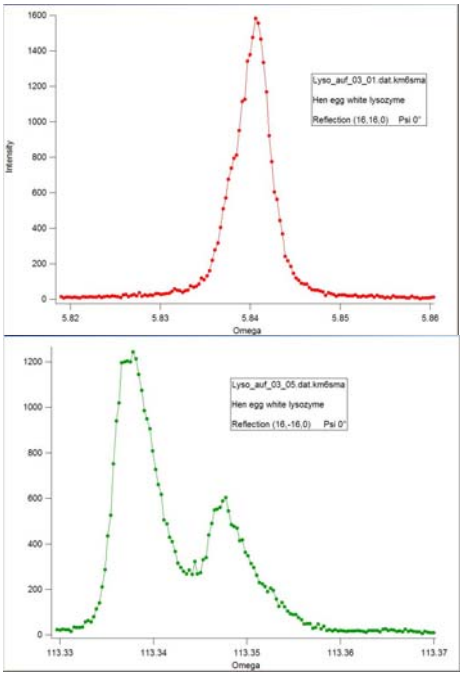

Fig. 2 Rocking curve measurements of the (16,16,0) and (-16,-16,0) reflections in the same crystal of hen egg-white lysozyme.

particular crystal quickly revealed the poor quality in certain orientations (see Fig. 2).

Authors : **D. Luebbert, A. Meents, and E. Weckert,** Hasylab. *Publication in preparation*

SYNCHROTRON AND PRECESSION ELECTRON DIFFRACTION FROM COHERENT NANO-SIZED Al -Zn-Mg PARTICLES IN AN ALUMINIUM MATRIX

Precipitate phases occur in many important commercial metallurgical systems as tiny semi-coherent particles dispersed in a matrix. Age-hardening aluminium alloys are prime examples. The precipitation sequence in the age-hardening Al-Zn-Mg system may be summarized as:

$$\text{Solid Solution} \rightarrow \text{GP-zones} \rightarrow \eta' \rightarrow \eta\text{–}MgZn_2$$

For the equilibrium phase, η-$MgZn_2$, structure determination has previously been done from X-ray single crystal work. Large single crystals cannot be synthesised for the other zones or for the metastable η' phase in the sequence, and therefore only structural models exist for these systems. For commercial applications of Al-Zn-Mg alloys, for example in the automotive industry for shock absorption, a fine dispersion of the metastable η'-phase in an Al matrix provides a considerable strengthening of the alloys - yield strengths comparable with steels can be achieved. Both from this technological aspect and from an academic point of view, crystal structure determination of the η'-phase is of great interest. The η' precipitate forms as discs with approximate thickness 5nm and diameter 15nm. The unit cell, which is hexagonal with lattice parameters a = 4.96 Å and c = 14.02 Å, is strictly

related to and has a certain orientation relationship to the aluminium matrix. It is because of the orientation relationship that it is possible to collect average intensities from a large number of precipitates in a single aluminium grain by single crystal techniques. But the crystal structure analysis of the η′-phase has several complications: the orientation relationship will lead to extensive overlap between precipitate and matrix reflections, which results in an incomplete data set; faults are frequent and compositions and density are not known.

A group from Stavanger University has collected three-dimensional data sets using both synchrotron data collected using the MAR-image plate at SNBL BM01A, and data collected using the novel precession technique in transmission electron microscopy. Figure 1 shows a comparison of the reconstructed [112] Al projection collected using synchrotron radiation (a) and the same projection reproduced using the precession technique (b). The benefit of the intensity data collected from synchrotron radiation is their kinematical nature and that they can be corrected by standard routines for e.g. absorption, polarization and Lorenz factor, in order to obtain high quality data. These may be subsequently used for e.g. refinement of the η′-structure and as basis for accurate quantitative phase characterization. The benefit of the precession technique in the electron microscope is that data can be collected from very small grains as appearing in industrial alloys. Based on intensities data sets both from synchrotron and precession technique, Patterson sections have been calculated and used as a guide for establishing new structure models for the meta-stable η′-phase. Patterson sections calculated from synchrotron data confirm sections based on electron diffraction data, and the suggested structure model is thereby improved. Further applications of synchrotron radiation in studies of the industrially important alloys may be characterisation of diffuse scattering in order to understand the decomposition reaction from solid solution to GP-zones, and to establish a better model for these zones. From an industrial point of view, great interest is related to phase distributions in alloys when different parameters are altered, such as chemical compositions, and vacancy/dislocation structure as a function of age hardening temperatures.

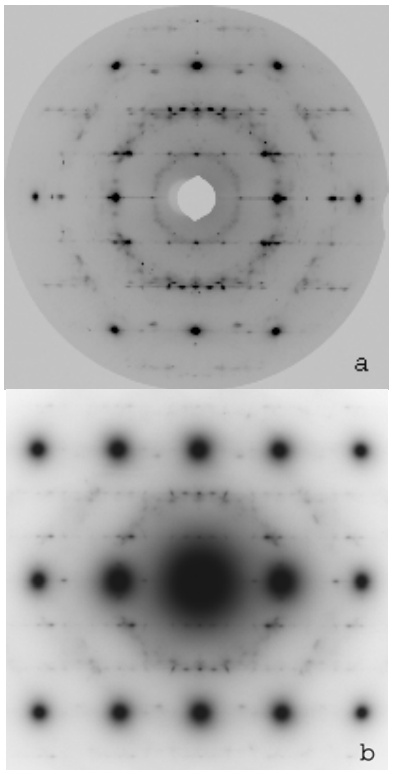

Fig. 1 Single crystal diffraction diagrams from a single aluminium grain orientated in [112] Al with η′ precipitates: a) Reconstructed from synchrotron X–ray diffraction of the reciprocal space. b) Projection taken with the electron diffraction precession technique.

Authors : **Kverneland A., Hansen, V., Larsen, H.B., Thorkildsen, G.**, University of Stavanger, **Pattison, P.**, SNBL, **Vincent, R.**, University of Bristol and **Gjønnes, J.**, University of Oslo. *Publication in preparation.*

COMBINING POWDER DIFFRACTION DATA FROM AREA DETECTOR AND HIGH RESOLUTION DIFFRACTOMETER FOR STRUCTURE SOLUTION AND REFINEMENT

Many small molecules which are liquid or gaseous at room temperature reveal several interesting crystalline phase transitions at low temperature. The ESRF powder diffraction group has developed the technique of inserting the liquid or gas into a capillary and recording the powder diffraction diagram of the frozen material as a function of temperature in a cryostat or N_2 gas cryostream. It has been possible to solve many new structures using this technique, in combination with powerful new software tools such as DASH or FOX. However, in some cases, the process of crystallization within the confines of a capillary produces powders with considerable texture or preferred orientation. When the powder diagram on a highly textured sample is collected using a high resolution diffractometer, the limited axial opening angle accepted by the diffractometer can result in unreliable measured intensities. This problem can be overcome by using an area detector for collecting reliable intensities, while using the high resolution diagram for establishing the correct lattice symmetry and space group. Since we have the MAR345 area detector available at SNBL, we have formed a collaboration with the ESRF powder diffraction group to exploit the possibilities provided by this combination of techniques.

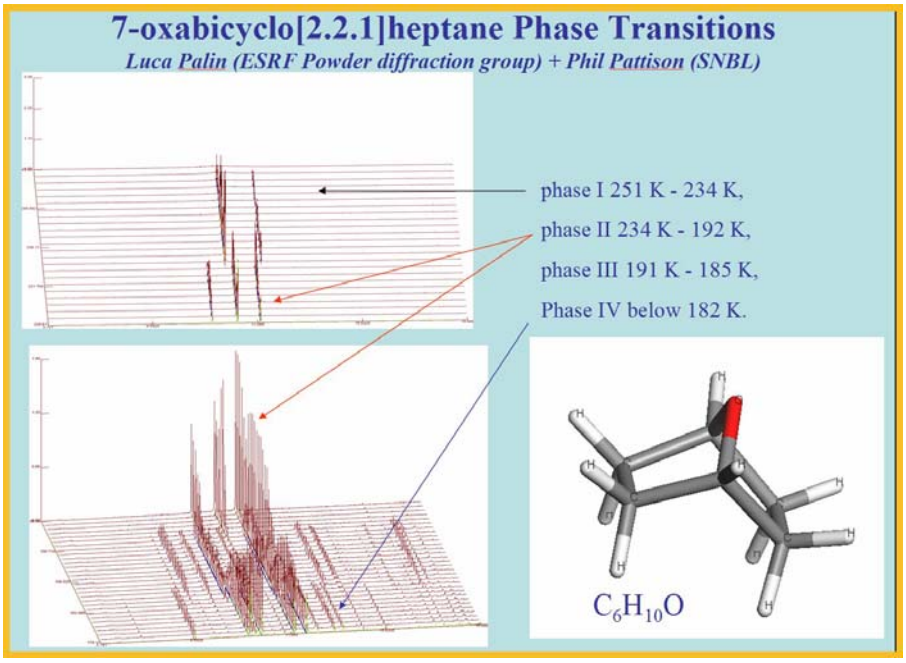

Fig. 1 Molecular structure of 7-oxabicyclo[2.2.1]heptane, and overview of the low temperature phases.

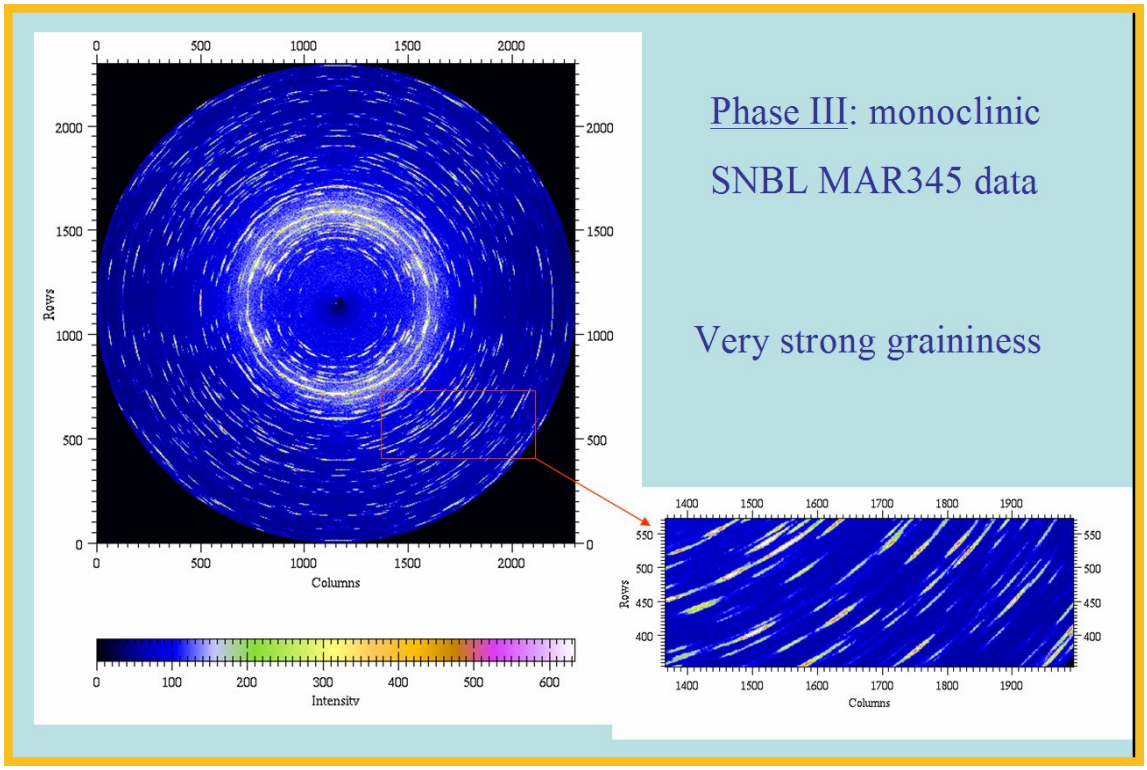

Fig. 2 Area detector images from BM1A of the Phase III of 7-oxabicyclo[2.2.1]heptane

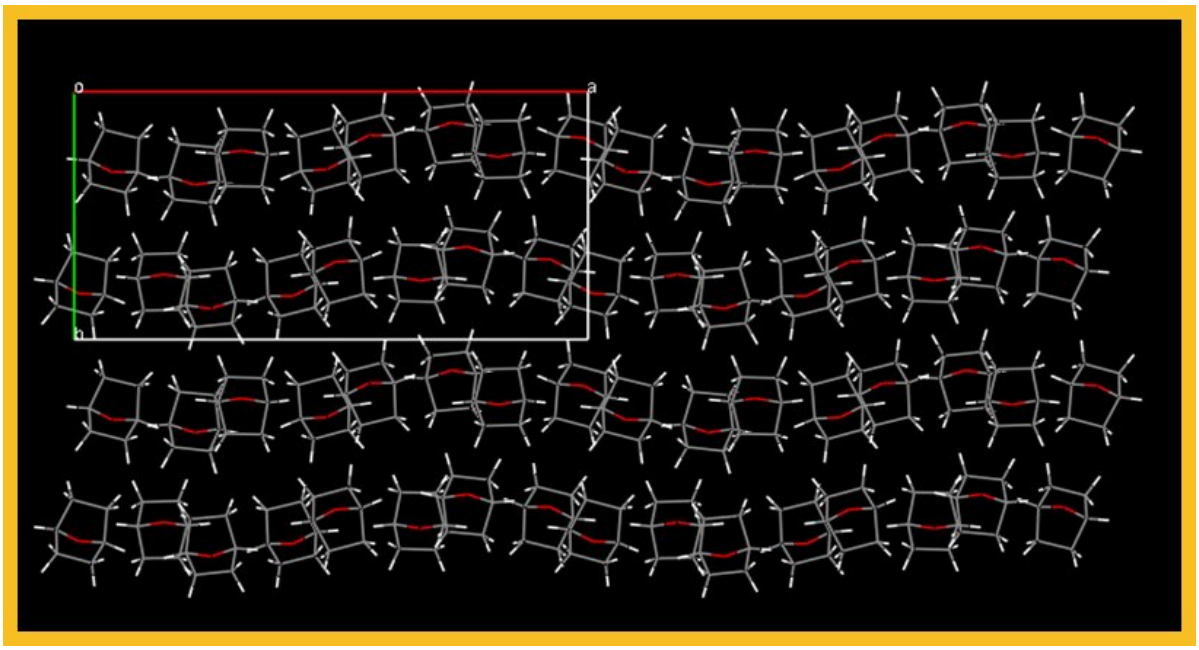

Fig. 3 Refined structure of the Phase III form of 7-oxabicyclo[2.2.1]heptane

The molecule which we have investigated as a starting point for this project is 7-oxabicyclo[2.2.1]heptane $C_6H_{10}O$, which shows four different crystalline phases below 251K. The molecular structure of this system and the behavior of the low temperature phases are illustrated in Fig. 1.

The high resolution powder data collected on BM16 for Phase III could be readily indexed to a monoclinic cell of space group $P2_1/a$ with a = 21.849(1) Å, b = 10.9664(4) Å, c = 9.3301(4) Å, β= 90.441(4)° and Z = 16, Z′ = 4. However, the intensities collected at high resolution proved to be unreliable for structural solution. The data were collected again on Phase III using the MAR345 image plate on BM1A. A glance at the strong texture and grainy powder pattern shown in Fig. 2 reveals immediately the problems faced by the high resolution technique. Without a reasonable full coverage of reciprocal space, the intensities in the powder pattern will clearly be inaccurate.

Despite the fact that the angular resolution in the image plate data is clearly significantly worse than the data collected with the analyzer crystal set-up on BM16, the intensities are much more reliable. This unknown crystal structure was solved from the MAR345 data using the program FOX, revealing four independent molecules in the unit cell. The solution could then be refined with GSAS, yielding the following R-factors: R_{wp}=8.45%, R_p=6.21% χ^2=3.86. The final structure solution is shown in Fig. 3.

Authors: L. Palin, P. Pattison (Grenoble, Lausanne).

APPLICATION OF A TEXTURE APPROACH TO STRUCTURE SOLUTION USING DATA IN TRANSMISSION MODE

Many compounds form only very small crystallites in the solid state. The technique of powder diffraction is then the method of choice to reveal the crystal structure. Unfortunately, even with the benefit of very high angular resolution available on the powder diffractometer at SNBL, complex structures with large unit cell dimensions may not be amenable to structure solution from powder data. The crucial problem is to resolve individual reflections, which overlap in a conventional powder diagram. Without the clear and unambiguous resolution of neighbouring reflections, it is not possible to partition the intensities correctly and therefore all efforts at structure solution are likely to fail.

The texture method is an experimental approach to resolving reflections. If the sample consists of crystallites, which can be aligned with some degree of preferred orientation, X-ray data can be collected which resemble a single crystal diffraction pattern. The method was first implemented in reflection mode using the high resolution diffractometer on SNBL (T.Wessels et al., *Science* **284** 1999 pp 477-479), and the same technique has now been developed for the transmission geometry. The experimental geometry is illustrated in Fig. 1, whereby the diffraction pattern is measured using the MAR345 image plate detector on BM1A. In the example used as a test case for the method, a total of 72 frames were collected in steps of 5° rotation per frame. Each of the 72 images was then divided into 18 radial wedges per quadrant, corresponding to a 5° tilt of the sample for each wedge.

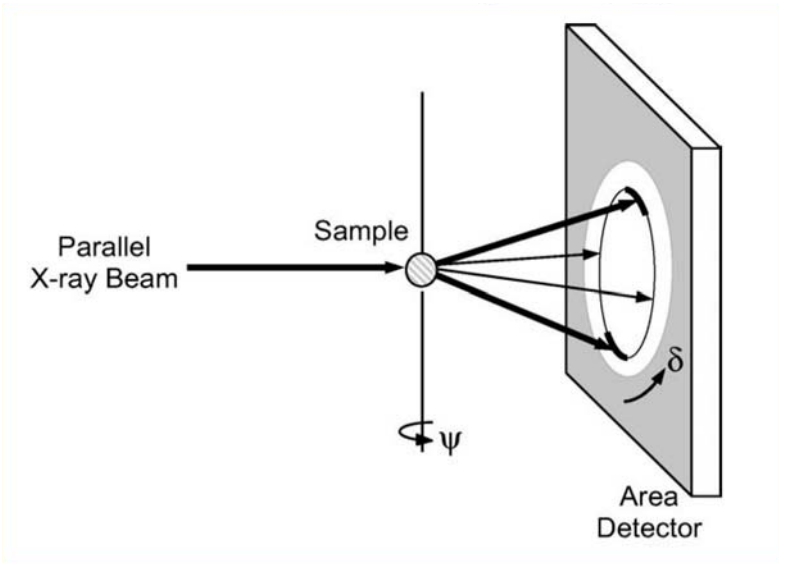

Fig.1 Experimental set-up for measurement of a textured sample in transmission mode

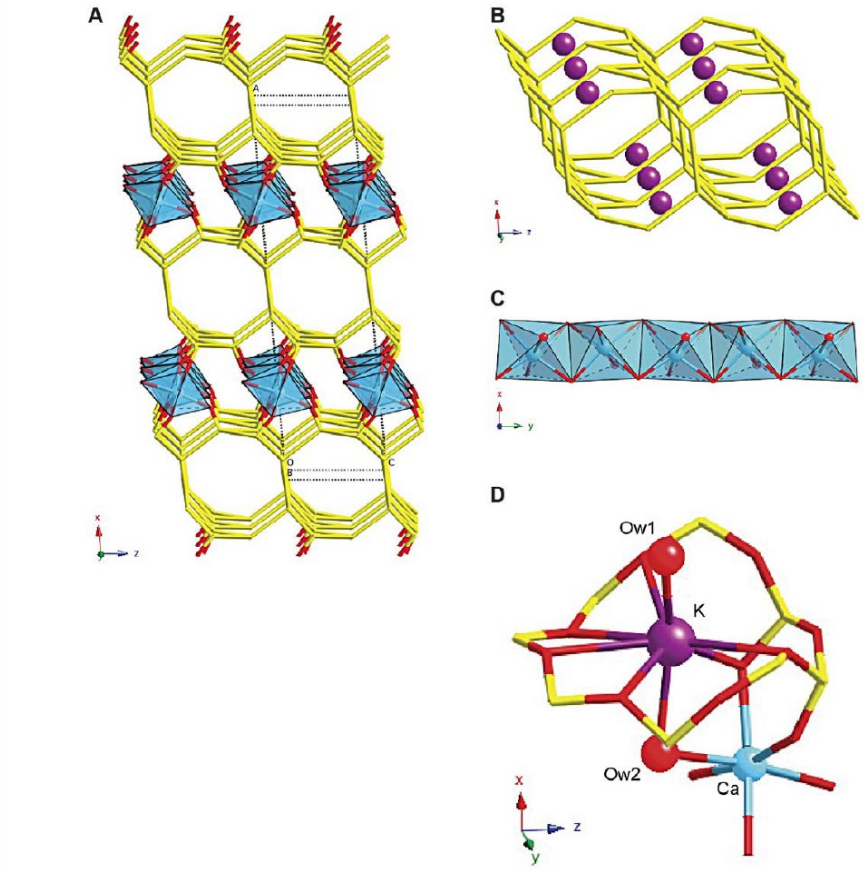

Fig. 2 The crystal structure of CAS-1 ($Ca_4K_4(H_2O)_8[Si_{16}O_{38}]$

Hence a total of 72 x 18 = 1296 diffraction patterns were generated, where each pattern can be associated with a different orientation of the sample. First the orientations of the crystallites (orientation distribution function) were determined by evaluating how the intensities of non-overlapping reflections change as a function of sample orientation. Then this information was used to calculated how much of the total intensity for each reflection would be observed for each sample orientation. In this way, reflections, which appear at a similar scattering angle can still be distinguished from one another, because their intensities will be concentrated in different parts of space.

The crystal structure of the potassium calcium silicate material, CAS-1 ($Ca_4K_4(H_2O)_8[Si_{16}O_{38}]$, has been determined from synchrotron radiation powder diffraction data, as an example of the newly developed texture approach to structure solution. First the orientation distribution function was determined using ten non-overlapping reflections. Then a set of intensities was extraction for all reflections, and used as input into a Direct Methods package for structure solution (SHELXS). A possible solution was found; the assignment of atoms made on the basis of the known chemical composition and ^{29}Si NMR spectrum, and the resulting structure was used as a starting point for Rietveld refinement. The refinement was carried out on a high resolution powder diffraction pattern collected on BM1B, thus illustrating nicely the advantages of having access to a combination of powder diffractometer and area detector on the same beamline. The refinement proceeded smoothly and the resulting structure is illustrated in Fig. 2.

Publication : J. L. Jorda et al. Comptes Rendus Chimie **8** (2005) 331.

STATUS OF FACILITY

BM1A: SINGLE CRYSTAL DIFFRACTOMETER AND LARGE AREA DETECTOR

P. Pattison

Operation

A total of approximately 800 shifts of beamtime were allocated to peer-reviewed research projects at BM1A during the last 24 months. The most serious disruption of 12 shifts was due to problems with the operation of the MAR345 image plate detector. The detector was returned to the manufactures (MarResearch GmbH, Hamburg) for a complete refurbishment, and is now fully operational. The shortage of staff over the last 12 months has let to some delays in the scheduling of experiments. We have now recruited an experienced crystallographer as a second beamline scientist, and are able to work our way through the back-log of experiments.

Both the MAR345 and the new CCD area detectors were in heavy demand by our user groups. The CCD is best optimised for rapid data collection aimed at single crystal structure solution and refinement. By switching from the MAR345 to the CCD, the average time for a high quality data collection has been reduced from 3 – 4 hours down to 1 -2 hours. The larger area of the MAR345 is still well-suited for investigating very large unit cell materials, for powder diffraction studies and for the measurement of diffuse scattering.

Technical status

The commissioning of the new CCD detector on the KM6 diffractometer has been successfully completed. Many individual data sets have been collected, and the first publications using these data are in print. The combination of CCD and point detector has also been invaluable for those experiments, which require a combination of fast data collection or crystal orientation together with precise monitoring of crystal quality with rocking curve measurements. The Helijet low temperature device has been used several times during the last 12 months, and the data are now being evaluated. Experience has shown that the persistent ice problems met earlier can be overcome with appropriate precautions.

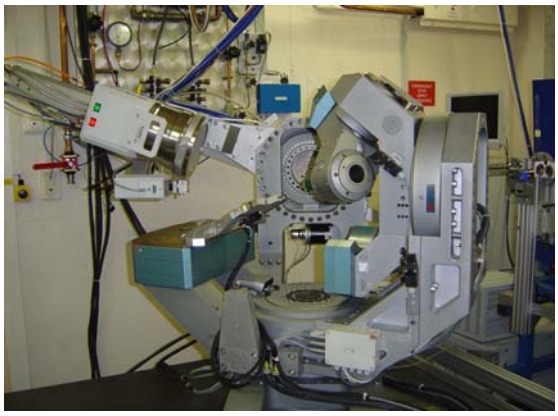

Fig. 1 The multi-axis KM6 single-crystal diffractometer, with its new CCD detector

The combination of movements available on the KM6 allows us to position the sample in an arbitrary orientation relative to the incoming synchrotron beam (and hence also to its polarization vector), and also to choose freely the angular coordinates of either of the X-ray detectors. This instrument now provides a completely generalized platform on which to

collect diffraction data. It can be configured either as a vertical or as a horizontal diffractometer, or indeed anywhere in between these scattering planes. Complete surveys of reciprocal space can be rapidly completed using the area detector, while the point detector provides the opportunity to investigate the profiles of individual reflections with high angular resolution. Information concerning the crystal orientation matrix and the diffractometer parameters can be passed smoothly from point detector to area detector configurations.

The SNBL team is currently developing a software model of the KM6 diffractometer in collaboration with the manufacturers (Oxford Diffraction Ltd) and a group from the University of Stavanger, Norway. The Stavanger group has already exploited the capabilities of the diffractometer to investigate the phenomenon of multiple beam diffraction in single crystals, and to elucidate the complex interactions between crystal quality, incident beam polarization and sample absorption. It is now our intention to include their theoretical model in the control software of the diffractometer, and to extend the existing controls to facilitate data collection in arbitrary scattering planes (the so-called “generalized diffractometer model”). This upgrade of the software and controls will allow experiments such as three-beam interference measurements to be carried out in a routine and straightforward manner. This will permit non-specialists to exploit multiple beam interference in order to determine, for example, absolute structures of chiral crystals. In addition, data collection in an arbitrary diffraction plane can greatly facilitate the use of sample environmental stages (e.g. diamond anvil cells) in single crystal experiments, where the limited opening angle of the cell can be a very serious handicap. Use of a generalized diffractometer model in our control software will allow the area detector to be positioned in an arbitrary orientation relative to the incoming beam, which can dramatically increase the amount of reciprocal space seen by the detector.

One of the goals of modern crystallography is to provide complete structural models, which can explain the complex and rich diffraction patterns often observed from “real” crystals. The recorded data may include diffuse scattering and incommensurate satellite reflections as well as Bragg reflections from one or more crystals in the sample. Some of these X-ray scattering features may be extended in reciprocal space and often highly anisotropic, while others are extremely sharp and require excellent angular resolution. The instrumentation which we have assembled on BM1A is, we believe, ideally suited to address these problems. We are also in the fortunate situation that our users in Norway and Switzerland include groups who have specific expertise in the relevant fields of data collection strategies, data analysis and modelling. One of the most fruitful developments, for example, is to be able to reconstruct the complete, three-dimensional reciprocal space information from a series of individual diffraction images recorded with an area detector.

BM1B: HIGH RESOLUTION POWDER DIFFRACTOMETER AND EXAFS SPECTROMETER

H. Emerich

A total of approximately 800 shifts of beamtime were allocated to peer-reviewed research projects at BM1B during the 24 months. Almost no beamtime was lost due to failure of beamline or station equipment. The most serious disruption was due to component failure in the monochromator, which could be repaired by the staff in less than two days. The general trend towards technically more and more complex experiments has continued. Operation of the powder diffractometer at photon energies around 30 – 35 keV has become routine, and the data quality for heavily absorbing samples (e.g. intermetallic hydrides) has improved as a result of access to the higher energy synchrotron beam. The demand for dedicated *in-situ* equipment, such as specialist gas lines and reaction vessels, has been increasing both for EXAFS and powder diffraction experiments.

In parallel to the daily work load of preparing and carrying out ever more complex experiments the beamline staff has been heavily involved in restructuring the beamline.

Technical Changes and Upgrades

After more than 10 years of daily operation considerable efforts are underway to keep the station state of the art. This holds especially for the EXAFS technique where it has also been pointed out by the beam line review committee last year (2004) that improvements should be undertaken to maintain the beamlines competitive edge. Improvements are targeted towards: challenging *in-situ* experiments, flux enhancement, glitch reduction (monochromator), combination of various measurement techniques (PD, EXAFS, Raman etc.). These improvements are integrated into an ongoing program, which can be summarized as follows:

A) Modifying the infrastructure of the SNBL stations, to host additional equipment.
B) Installation of new beamline components and detectors; improvements on the sample environment.
C) General refurbishment of the station and the data acquisition room.

A) Modifying the Infrastructure of the BM1B Station.

Those that have been using the station over the years have certainly noticed that the available space in the B-station became increasingly scarce. Having in mind that more equipment is needed to keep the station at the state of the art a major change of the station became necessary. Therefore we concentrated a major part of the SNBL staff activities in 2005 onto the preparation and the realization of theses changes which have been accomplished recently.

The present situation can be summarized as follows: all vacuum vessels formerly placed in the B-station have been moved upstream and are now located in the optics enclosure. Notably: the monochromator, the in-vacuum secondary slits, the Be-window and the white beam stop together with their respective vessels and support stands have all been

taken out from the station and moved into the optics enclosure. The move involved an almost complete redesign of most of the involved beamline components. It is noteworthy that the removal of all these beamline components in the B-hutch is also expected to reduce the X-ray background for noise sensitive experiment.

B) Installation of New Beamline Components.

The activities described above serve only to create the necessary space for the installation of additional beamline components and equipment to enlarge the possibilities connected to the sample environment.
For the beamline components the following changes have been carried out or are envisaged:

B1) Installation and Commissioning of a 13 Element Solid State Detector

One important recent improvement has certainly been the acquisition of a 13 element solid state detector together with its integration into the existing EXAFS set-up in 2004. With the necessity to run a calibration program and the need to cater for various output file formats it was already clear from the start that the acquisition software used hitherto was not compatible with the requirements for the solid state detector.

Fig. 2 View of the BM1B station before, during, and after the changeover.

It was therefore decided to follow the ESRF example and to use Spec as control software for the EXAFS scans. In order to carry out these software changes a technical trainee was hired for a year and, together with the help of the ESRF software group (BLISS), the first experiments using the new detector could be given out to the users by autumn 2004. The detector is now in routine operation, and has been used successfully by several groups. The 13 channels of this detector permit a dramatic improvement in the sensitivity of the EXAFS measurements on very dilute samples. This improvement has a big impact on the possibilities for investigating environmentally important, low concentration samples, as well as metallo-proteins.

Figure 3 show EXAFS scans at the Ru edge carried out in fluorescence mode.

The following changes are in preparation or at least in a planning stage:

B2) Acquisition and Integration of a Liquid-He Flow Cryostat.

After the complete breakdown of our "old" cryostat many of our users had to face the difficult situation that experiments below Liquid-N_2 temperatures where not possible anymore on BM1B. The availability of a cryostat allowing access down to 4 K is a vital part of the equipment for SNBL since a large fraction of our users frequently need low temperatures, either to study phase transitions at cryogenic temperatures, or in order to reduce the thermal atomic motion (Debey-Waller factor) for very sensitive experiments.
Open space around the beam is limited

Fig. 3 The 13-element detector

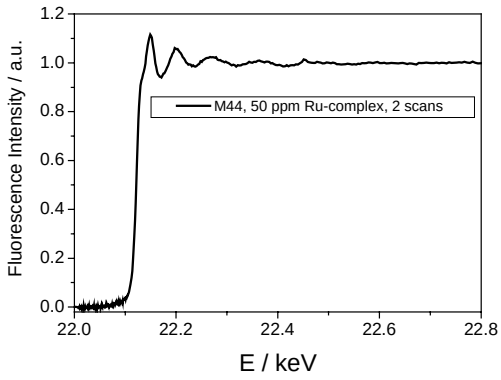

Fig. 4 Ru K-edge EXAFS scan of 50 ppm Ru in solution

due to the presence of the beam pipe for the A-line all through the hutch, therefore no off-the-shelf solution could be chosen. Furthermore, driven by the desire to have a device working for both: EXAFS and powder diffraction experiments (even simultaneously if needed), together with the need to allow for sample rotation at any temperatures a purpose tailored design had to be developed.

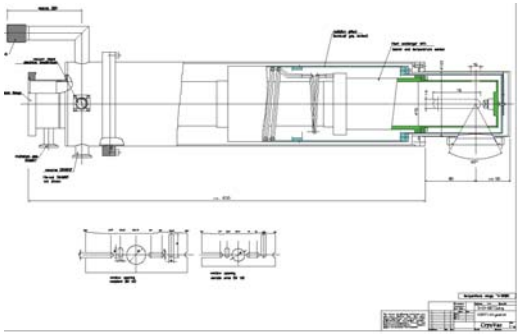

Fig. 5 Technical drawing of the cryostat

Since funding is now assured we can move ahead and an order for a new cryostat is about to be placed. The new design should allow for powder diffraction experiments either with a 2D detector or the existing powder diffractometer. Furthermore we think that EXAFS experiments in transmission mode and/or in fluorescence mode or even combined EXAFS/Powder experiments at very low temperatures will become possible. Last, but not least, the possibility to perform rapid sample changes ("cold swaps") is expected to reduce the loss of beam time due to the now unnecessary heating/cooling cycles involved.

B3) Upgrading to a Full Two Crystal Monochromator

Especially our EXAFS community is in need of a detunable double crystal monochromator. We are planning for a system allowing changing between a first set of two Si [111] crystals for high flux, and a second set of Si [311] crystals when high resolution is needed. We expect a substantial reduction in the number and intensity of the glitches currently spoiling our EXAFS data by adding a piezo driven active feed back system to the second reflecting crystal. The design work for this upgrade is presently carried out by the beamline staff. Thanks to the help of a technician detached from the University of Trondheim, Norway, for that very purpose we are now in a situation where we have the necessary manpower to kick-start this project.

B4) Installation of a Collimating & Focusing System for EXAFS and Powder Diffraction

In the past we could only use a part of the beam for most of the experiments carried out on SNBL. With the recent changes the B-line is now set up to receive 1 mrad of beam from the ESRF bending magnet source. It is obviously highly desirable to recover these valuable photons for experiments that allow doing so. We therefore consider the option of buying a cylindrical mirror, since the space, which has just been created, would allow for the installation of such a device.

B5) Development of a „Mini - Focus" Device

Being able to measure individual small crystallites is a recurring demand on SNBL. Recent examples are powder measurements on a small natural Zeolite, a very limited amount of sample grains or the investigation of the strain field around hard metal grains held in a ductile matrix.
Several prototypes for mild focusing have already been developed and successfully tested by the SNBL staff members. The recent acquisition of a used CNC milling machine from the ESRF, together with the recently created space on the beam line should allow for a long awaited mini focus device to materialize. We hope to be able to develop a system allowing focusing a beam from 1–2 mm down to roughly 150 μm once the work linked to the new monochromator has been completed.

C) General refurbishment of the station and the data acquisition room

After more than 10 years of extensive use the appearance of the beamline shows signs of wear. Although this point is of minor importance for the functionality of the station, it is desirable to create a positive working ambiance. Therefore we intend to improve the appearance of the station by getting the floor and wall covers remade, together with the infrastructural changes described below.
These "embellishments" will be carried out by external companies during shutdown periods without any loss in beam time. Additional functional changes to the infrastructure on the beamline, such as the installation of stainless steel gas supply lines and electrical distribution panels, are intended to be carried out at the same time.

Future Developments

Besides the technical changes described above the beam line staff still pursues the evaluation of utilizing a Raman spectrometer in combination with powder diffraction/EXAFS *in-situ* experiments started last year. Several additional combined x-ray/Raman measurements are in preparation and we are presently negotiating the loan of a Raman spectrometer for these experiments.

ANCILLARY EQUIPMENT AND ENVIRONMENTAL STAGES

The SNBL beamlines posses a variety of ancillary equipment and environmental stages for high and low temperature experiments, as well as high pressure X-ray diffraction. In addition, SNBL participates in the ESRF loan pool arrangement, providing access to detectors, electronics and sample environment stages. Amongst the equipment owned directly by SNBL are an Oxford Cryostream N_2 cooler (90K – 370K) and an Oxford Diffraction Helijet (10K – 90K). In additional, we have a Cyberstar Heater/Blower system allowing temperatures up to 1300 K to be reached. An in-house furnace can accommodate spinning samples up to a temperature of 1100 K. For EXAFS and powder diffraction experiments, we also have specialist sample cells for *in-situ* experiments, gas mixtures, dehydration and hydrogenization processes etc. A special heater designed by the ETH Zurich has been purchased for the MAR345 detector system, and allows us to reach temperature of 1200 K for temperature dependent single crystal experiments and studies of diffuse scattering.
In addition to the local sample environments, we also have an off-line spectrophotometer for optical absorption experiments. The spectrometer has been specifically designed for optical measurements on single crystals mounted on a standard goniometry head. This allows us to monitor periodically the effects of radiation damage in crystals, for example, or to follow the progress of photo-activated transformations in solid-state photochemistry experiments.

The high pressure powder diffraction experiments, which are also, carried out on BM1A employ a narrow,

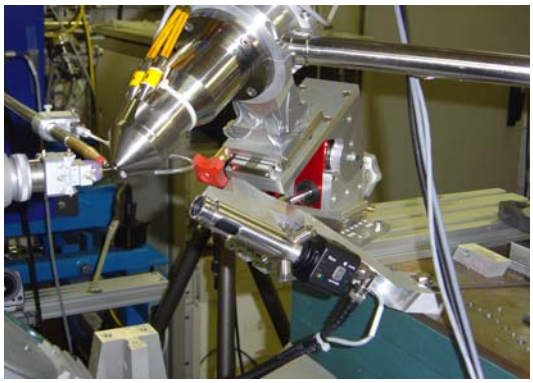

Fig.6 The Helijet helium cooling device mounted on the KM6 diffractometer

Fig.7 The set-up for alignment and calibration of high pressure experiments on the MAR345 area detector.

monochromatic focused synchrotron beam, reduced by precision slits down to a cross-section of about 50 microns. This beam must be carefully aligned relative to the diamond anvil cell in order to avoid scattering from the gasket material. An optical microscope and precision alignment stage are shown, together with a ruby laser line for pressure calibration.

FACTS AND FIGURES

Administration and Finance

Ch. Heurtebise

The SNX Foundation was officially established in January 2004, its seat being in Lausanne (Switzerland). The SNX Foundation allows the SNBL to have their own accounting and administrative operations, dealt with by the Administrative Manager. All the transfers of funds are done via the SNX bank accounts. Three bank accounts were opened, one which receives the funds according to contract from NSR (Norway), one which receives funds according to contract from SER (Switzerland), and a third account for funds outside contract, from any Swiss or Norwegian institutions, university etc.
An Association (Assosiation Suisse-Norvégienne Grenoble) has been founded, end of December 2004, by the SNX Foundation, to employ staff in France. The scope of the ASNG is to provide services and technical expertise for the daily running of the SNBL.
The SNX Foundation and ASNG are a real means of saving time and money of the administrative side, and is a means of directly implying all the staff in optimizing the use of the funds.

BUDGET (in CHF)

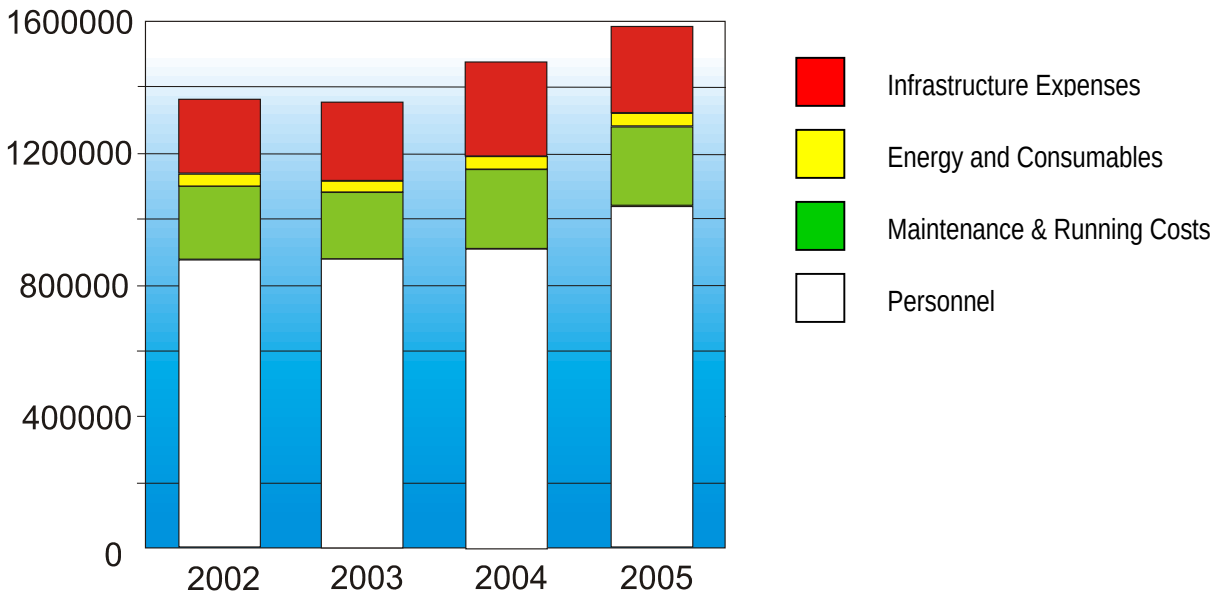

BUDGET in CHF	2002	2003	2004	2005
Personnel	880,083.00	878,829.60	913,150.00	1,036,944.00
Maintenance and Running Costs	220,883.00	199,684.00	240,000.00	240,000.00
Energy and Consumables	37,805.00	34,884.00	35,000.00	35,000.00
Infrastructure Expenses	223,142.00	238,112.40	287,731.00	275,186.00
TOTAL	**1,361,913.00**	**1,351,510.00**	**1,475,881.00**	**1,587,130.00**

INCOME (in CHF)

Income Outside Contract

Income According to Contract

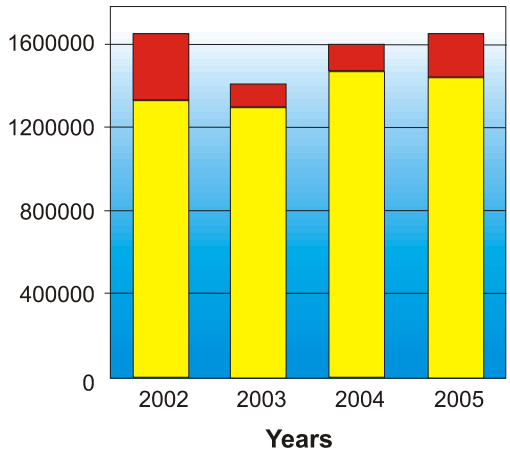

INCOME in CHF	2002	2003	2004	2005
Income According to Contract	1,332,638.00	1,293,720.00	1,475,000.00	1,450,000.00
Income Outside Contract	312,341.00	114,948.00	123,379.00	194,887.00
TOTAL	**1,644,978.00**	**1,408,668.00**	**1,598,379.00**	**1,644,887.00**

EXPENDITURE (in CHF)

Infrastructure Expenses

Energy and Consumables

Maintenance & Running Costs

Personnel

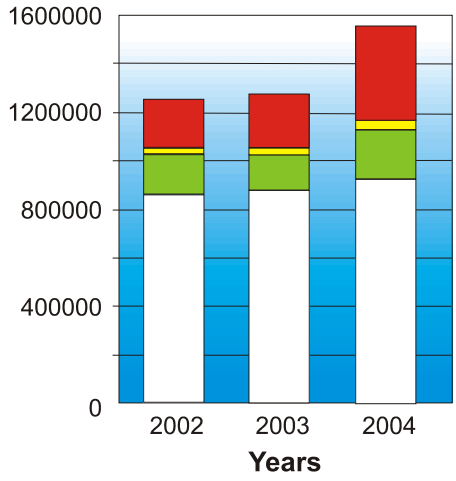

EXPENDUTRE in CHF	2002	2003	2004
Personnel	868,983.35	874,264.52	930,478.57
Maintenance and Running Costs	164,153.73	153,745.73	198,002.00
Energy and Consumables	25,056.80	28,663.82	45,496.00
Infrastructure Expenses	199,937.15	224,339.96	388,455.87
TOTAL	**1,258,517.79**	**1,281,014.03**	**1,562,432.44**

PUBLICATIONS

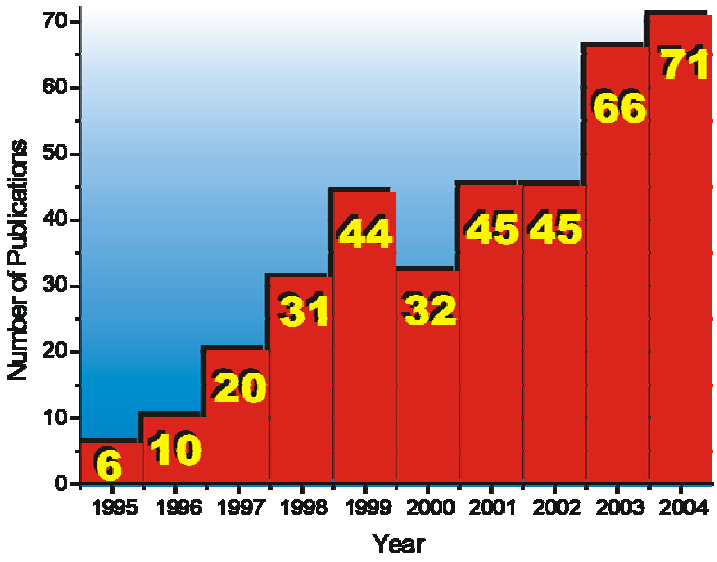

Publication Rate since start-up of SNBL

The *Journal Citation Report* provides quantitative tools for ranking, evaluating, and comparing journals publishing scientific results. The ***impact factor*** is one of these; it is a measure of the frequency with which the "average article" in a journal has been cited in a particular year of period. The most important and recent use of IF is in the process of academic evaluation. We have chosen IF to characterize the impact of the papers recently published by the SNBL users as the other indices, like Citation Index, due to a short-range time scale, do not reflect their real scientific "weight".

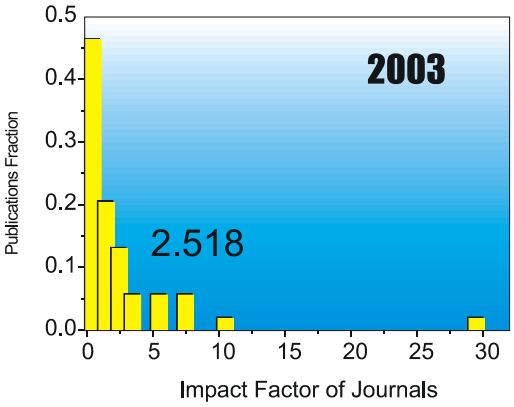

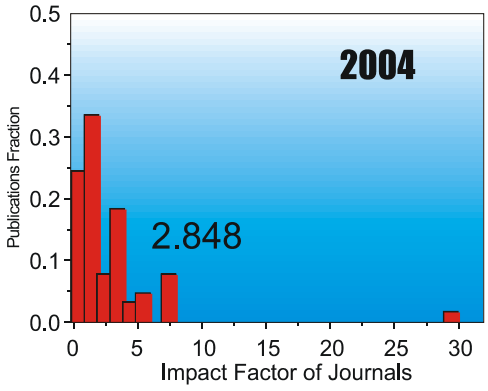

One notices, from the Figures, a shift of the "average SNBL publication" towards the journals with higher IF, a sign of the increasing quality of the papers published by the SNBL users. The increase is characteristic for all years of the SNBL operations.

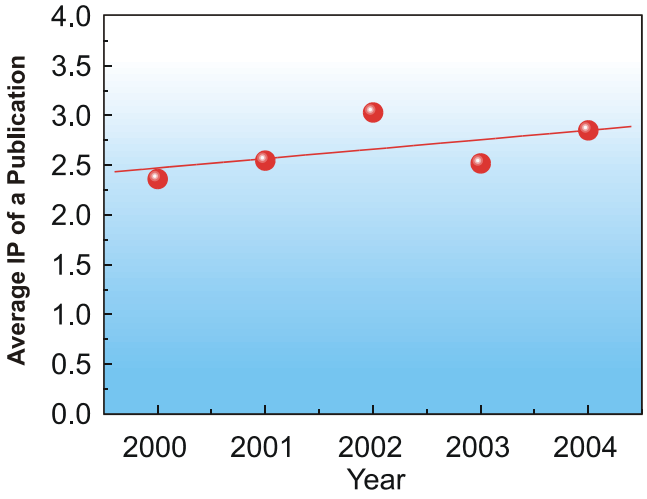

Impact factor of the “average journal” for a paper produced by the SNBL Users. Straight line is the best least-square fit.

List of Publications

2003

1. Andersen, O.L., Stokka, A.L., Flatmark, T., Hough, E. 2.0 A Resolution crystal structures of the ternary complexes of Human phenylalanine hydroxylase catalytic domain with tetrahydrobiopterin and 3-(2-thienyl)-L-alanine or L-norleucine: substrate specificity and molecular motions related to substrate binding *J. Mol. Biol.*, 333, 747-757, 2003
2. Arakcheeva, A., Chapuis, G., Birkedal, H., Pattison, P., Grinevitch, V. The commensurate composite of sigma-structure to beta-tantalum, *Acta Cryst.*, B59, 324-336, 2003
3. Birkedal, H., Van Beek, W., Emerich, H., Pattison, P. Thermal expansion and phase purity of commercial MgB_2, *J. of Materials Science Letters*, 22, 1069-1071, 2003
4. Bjork, A., Dalhus, B., Mantzilas, D., Eijsink, V.G.H., Sirevag, R. Stabilization of a tetrameric malate dehydrogenase by introduction of a disulfide bridge at the dimer-dimer interface, *J. Mol. Biol.*, 334, 811-821, 2003
5. Bodak, O., Tokaychuk, Ya., Manyako, M., Pacheco, V., Cerný, R., Yvon, K. Structural and magnetic properties of iron-rich compounds in the Yb–Fe–Al system, *J. of Alloys & Compounds*, 354, L10-L15, 2003
6. Boldyreva, E.V., Ashbahs, H., Weber, H.-P. A comparative study of pressure-induced lattice strain of and -polymorphs of glycine, *Z. Kristallogr.*, 218, 231-236, 2003
7. Boldyreva, E.V. High-Pressure studies of the anisotropy of structural distortion of molecular crystals, *J. of Molecular Structure*, 647, 159-179, 2003
8. Bonhoure, I., Wieland, E., Scheidegger, A.M., Ochs, M., Dunk, D. EXAFS study of Sn(IV) Immobilization by hardened cement paste and calcium silicate hydrates, *Environ. Sci. Technol.*, 37, 2184-2191, 2003
9. Brinks, H.W., Maeland, A.J., Hauback, B.C., Bowman Jr, R.C., Cantrell, J.S. Determination of deuterium site occupation in $Zr_4Pd_2OD_{4.5}$, *J. of Alloys & Coumpounds*, 361, 108-112, 2003
10. Brinks, H.W., Hauback, B.C. The structure of Li_3AlD_6, *J. of Alloys & Compounds*, 354, 143-147, 2003
11. Brinks, H.W., Hauback, B.C., Norby, P., Fjellvag, H. The decomposition of $LiAlD_4$ studied by in-situ X-ray and neutron diffraction, *J. of Alloys & Compounds*, 351, 222-227, 2003
12. Cerny, R., Alami-Yadri, K. Orthorhombic Yb_5Si_4 from synchrotron powder data, *Acta. Cryst.*, E59, i1/i3, 2003
13. Chernyshev, V., Machon, D., Fitch, A.N., Zaitsev, S., Yatsenko, A.V., Shmakov, A.N., Weber, H.-P. Protonation site and hydrogen bonding in two crystalline forms of doxazosin mesylate from powder diffraction data, *Struct. Chem.*, B59, 787-793, 2003
14. Chernyshov, D., Hostettler, M., Töernroos, K.W., Büergi, H.-B. Ordnungsphaenomene und phasenuebergaenge in einer spin-crossover-

verbindung: [Fe(2-pic)$_3$]Cl$_2$.EtOH durchlaeuft eine geordnete zwischenphase, *Angew. Chem*., 115, 3955-3960, 2003

15. Chernyshov, D., Hostettler, M., Töernroos, K.W., Büergi, H.-B. Ordering phenomena and phase transitions in a spin-crossover compound-uncovering the nature of the intermediate phase of [Fe(2-pic)$_3$]Cl$_2$.EtOH, *Angew. Chem. Int*., 42, 3825-3830, 2003

16. Cowan-Jacob, S.W., Kaufmann, M., Anselmo, A.N., Stark, W., Gruetter, M.G. Structure of rabbit-muscle glyceraldehyde-3-phosphate dehydrogenase, *Acta Cryst*., D59, 2218-2227, 2003

17. Dalconi, M.C., Alberti, A., Cruciani, G., Ciambelli, P., Fonda, E. Siting and coordination of cobalt in ferrierite: XRD and EXAFS studies at different Co loadings, *Microp. & Mesop. Mat*., 62, 191-200, 2003

18. Dalhus, B., Johnsen, L., Nissen-Meyer, J. Crystallization and preliminary X-ray data investigation of the bacterial enterocin A immunity protein at 1.65Å resolution, *Acta Cryst*., D59, 1291-1293, 2003

19. Dmitriev, V., Sinitsyn, V., Dilanian, R., Machon, D., Kuznetsov, A., Ponyatovsky, E., Lucazeau, G.et al. In situ pressure-induced solid-state amorphization in $Sm_2(MoO_4)_3$, $Eu_2(MoO_4)_3$ and $Gd_2(MoO_4)_3$ crystals: chemical decomposition scenario, *J. of Phys. & Chem. of Solids*, 64, 307-312, 2003

20. Dmitriev, V., Kuznetsov, A., Machon, D., Weber. H.-P., Tolédano, P. Phase transition mechanisms in lanthanide elemental crystals, *Europhys. Lett*., 61, 783-789, 2003

21. Dubrovinsky, L.S., Dubrovinskaia, N.A., Prakapenka, V., Seifert, F., Langenhorst, F., Dmitriev, V., Weber, H.-P. et al. High-Pressure and high-temperature polymorphism in silica, *High Pressure Research*, 23, 35-39, 2003

22. Dubrovinsky, N., Dubrovinskaia, N. A., Langenhorst, F., Dobson, D., Rubie, D., Gessmann, C., Abrikosov, I.A. et al. Iron-silica interaction at extreme conditions and the electrically conducting layer at the base of earth's mantle, *Nature*, 422, 58-61, 2003

23. Dubrovinsky, L.S., Dubrovinskaia, N.A., McCammon, C., Rozenberg, G. Kh., Ahuja, R., Osorio-Guillen, J.M., Dmitriev, V. et al. The structure of the metallic high-pressure Fe_3O_4 polymorph: experimental and theoretical study, *J. Phys.: Condens. Matter*, 15, 7697-7706, 2003

24. Goryainov, S.V., Boldyreva, E.V., Smirnov, M.B., Ashbahs, H., Chernyshev, V.V., Weber, H-P. Isosymmetric reversible pressure-induced phase transition in sodium oxalate at 3.8 GPa, *Doklady Physical Chemistry*, 390, 154-157, 2003

25. Grunwaldt, J-D., Maciejewski, M., Baiker, A. *In situ* x-ray absorption study during methane combustion over Pd/ZrO_2 catalysts, *Phys. Chem. Chem. Phys*., 5, 1481-1488, 2003

26. Guénée, L., Yvon, K. Synthesis, crystal structure and hydrogenation properties of the novel metal compound $LaNi_2Mn_3$, *J. of Alloys & Compounds*, 348, 176-183, 2003

27. Guénée, L., Favre-Nicolin, V., Yvon, K. Synthesis, crystal structure and hydrogenation properties of the ternary compounds LaNi4Mg and NdNi4Mg, *J. of Alloys & Compounds*, 348, 129-137, 2003

28. Guillou, N., Livage, C., Van Beek, W., Noguès, M., Férey, G. A layered nickel succinate with unprecedented hexanickel units: structure elucidation from powder-diffraction data, and magnetic and sorption properties, *Angew. Chem. Int*., 42, 643-647, 2003

29. Hoegbom, M., Galander, M., Andersson, M., Kolberg, M., Hofbauer, W., Lassmann, G., Nordlund, P. & al. Displacement of the tyrosyl radical cofactor in ribonucleotide reductase btained by single-crystal high-filed EPR and 1.4-A x-ray data, *PNAS*, 100, 3209-3214, 2003

30. Hostettler, M., Birkedal, H., Schwarzenbach, D. The yellow polymorphs of Mercuric iodide (HgI_2), *Helvettica Chimica Acta*, 86, 1410-1422, 2003

31. Jorda, J.L., McCusker, L.B., Baerlocher, C., Morais, C.M., Rocha, J., Fernandez, C., Borges, C. et al. Structure analysis of the novel microporous aluminophosphate IST-1 using synchrotron powder diffraction data and HETCOR MAS NMR, *Microp. & Mesop. Mat*., 65, 43-57, 2003

32. Karen, P. Effects of oxygen nonstoichiometry and of its distrubition on Verwey-type transitions and structure of $GdBaFe_2O_{5+w}$, *J. of Solid State Chem*., 170, 9-23, 2003

33. Kiener, C., Kurtz, M., Wilmer, H., Hoffmann, C., Schmidt, H-W., Grunwaldt, J-D., Muhler, M. et al. High-throughput screening under demanding conditions: Cu/ZnO catalysts in high pressure methanol synthesis as an example, *J. of Catalysis*, 216, 110-119, 2003

34. Khyzhun, O. Yu., Lototsky, M.V., Riabov, A.B., Rosenkilde, C., Yartys, V.A., Joergensen, S., Denys, R.V. Sn-containing (La,Mn)$Ni_{5-x}Sn_xH_{5-6}$ intermetallic hydrides: thermodynamic, structural and kinetic properties, *J. of Alloys and Compounds*, 356-357, 773-778, 2003

35. Kongshaug, K.O., Fjellvag, H. Novel coordination polymers based on nickel (II) and 2,6-

naphthalenedicarboxylate, *Solid State Sciences*, 5, 303-310, 2003

36. Kongshaug, K.O., Fjellvag, H. Synthesis and characterization of the mixed ligand coordination polymer CPO-5, *J. of Solid State Chem.*, 175, 182-187, 2003

37. Krauss, G., Miletich, R., Steurer, W. Reciprocal-space imaging and the use of a diamond-anvil cell: a single-crystal high-pressure study of a quasicrystal up to 10.7 GPa, *Philisoph. Magazine Letters*, 83, 525-531, 2003

38. Kuznetsov, A., Dmitriev, V., Bandilet, O., Weber, H.-P. High-temperature fcc phase of Pr: negative thermal expansion and intermediate valence state *Phys. Rev.*, B68, 064109, 2003

39. Leiros, I., Moe,, E., Lanes, O., Smalas, A.O., Willassen, N.P. The structure of uracil-DNA glycosylase from atlantic cod (Gadus morhua) reveals cold-adaptation features, *Acta Cryst.*, D59, 1357-1365, 2003

40. Machon, D., Dmitriev, V., Bouvier, P., Timonin, P., Shirokov, V., Weber, H.-P. Pseudoamorphization of Cs_2HgBr_4, *Phys. Rev.*, B68, 144104, 2003

41. Machon, D., Sinitsyn, V., Dmitriev, V., Bashkin, I., Dubrovinsky, L., Kuleshov, I., Ponyatovsky, E. et al. Structural transitions in Cu_2O at pressures up to 11 GPa, *J. Phys.: Condens. Matter*, 15, 7227-7235, 2003

42. Maehlen, J.P., Yartys, V.As., Hauback, B.C. Structural studies of deuterides of yttrium carbide *J. of Alloys & Compounds*, 351, 151-157, 2003

43. Maehlen, J.P., Yartys, V.A., Hauback, B.C. Structural studies of the deuterides of carbon containing yttrium alloys, *J. of Alloys and Compounds*, 356-357, 475-479, 2003

44. Maekelae-Vaarne, N.I., Nicholson, D.G., Ramstad, A.L. Supported metallocene catalysts-interactions of (n-BuCp)2$HfCl_2$ with methylaluminoxane and silica, *J. of Molecular Catalysis A: Chemical*, 200, 323-332, 2003

45. Martucci, A., Alberti, A., Guzman-Castillo, M. de L., Di Renzo, F., Fajula, F. Crystal structure of zeolite omega, the synthetic counterpart of the natural zeolite mazzite, *Microp. & Mesop. Materials*, 63, 33-42, 2003

46. Palosz, B., Grsanka, E., Stel'makh, S., Gierlotka, S., Pielaszek, R., Bismayer, U., Weber, H.-P. et al. Application of powder diffraction methods to the analysis of short- and long-range atomic order in nanocrystalline diamond and SiC; the concept of the apparent lattice parameter (alp), *Solid State Phenomena*, 94, 203-216, 2003

47. Palosz, B., Grsanka, E., Gierlotka, S., Stel'makh, S., Pielaszek, R., Lojkowski, W., Bismayer, U. et al. Application of x-ray powder diffraction to nano-materials - Determination of the atomic structure of nanocrystals with relaxed and strained surfaces, *Phase Transitions*, 76, 171-185, 2003

48. Paszkowics, W., Cerny, R., Krukowski, S. Rietveld refinement for indium nitride in the 105-295 K range, *Powder Diffraction*, 18, 114-121, 2003

49. Prakapenka, V.B., Dubrovinsky, L.S., Shen, G., Rivers, M.L., Sutton, S.R., Dmitriev, V., Weber, H.-P. et al. Alpha-PbO_2-type high-pressure polymorph of GeO_2, *Phys. Rev.*, B67, 132101, 2003

50. Renaud, J., Bischoff, S.F., Buhl, T., Floersheim, P., Fournier, B., Halleux, C., Kallen, J. et al. Estrogen Receptor Modulators: Identification and structure-Activity relationsiphs of potent Er-alpha-selective tetrahydroisoquinoline ligands, *J. Med. Chem.*, 46, 2945-2957, 2003

51. Renaudin, G., Bertheville, B., Yvon, K. Synthesis and structure of an orthorhombic low-pressure polymorph of caesium magnesium hydride, $CsMgH_3$, *J. of Alloys & Compounds*, 353, 175-179, 2003

52. Renaudin, G., Guénée, L., Yvon, K. $LaMg_2NiH_7$, a novel quaternary metal hydride containing tetrahedral $[NiH_4]_4$- complexes and hydride anions, *J. of Alloys & Compounds*, 350, 145-150, 2003

53. Riabov, A.B., Yartys, V.A., Denys, R.V., Hauback, B.C. $Zr_4Al_3D_{2.68}$ and $Zr_3Al_2D_{2.26}$: new Zr-containing intermetallic hydrides with ordered hydrogen sublattice, *J. of Alloys & Compounds*, 356-357, 91-95, 2003

54. Risnes, H., Fjellerup, J., Henriksen, U., Moilanen, A., Norby, P., Papadakis, K., Posselt, D., Sørensen, L. H. Calcium addition in straw gasification, *Fuel*, 82, 641-651, 2003

55. Roux, M., Marichal, C., Le Meins, J-M., Baerlocher, C., Chézeau, J-M. Solid state NMR and X-ray diffraction study of three forms of the aluminophosphate $AlPO_4$-ZON, *Microp. & Mesop. Mat.*, 63, 163-176, 2003

56. Schoenleber, A., Pattison, P., Chapuis, G. The (3+1)-dimensional superspace description of the commensurately modulated structure of p-chlorobenzamide (alpha-form) and its relation to the gama-form, *Z. Kristallogr.*, 218, 507-513, 2003

57. Siebold, C., Arnold, I., Garcia-Alles, L. F., Baumann, U., Erni, B. Crystal structure of the citrobacter freundii dihydroxyacetone kinase reveals an eight-stranded alpha-helical barrel ATP-binding domain, *J. Biol. Chem.*, 278, 48236-48244, 2003

58. Stange, M., Lindén, J., Kjekshus, A., Binsted, N., Weller, M.T., Hauback, B.C., Fjellvag, H.

Structural aspects of Pr_{1-x} ·Sr_xFeO_{3-w}, *J. of Solid State Chem*., 173, 148-163, 2003
59. Swamy, V., Dubrovinsky, L.S., Dubrovinskaia, N.A., Simionovici, A.S., Drakopoulos, M., Dmitriev, V., Weber, H.-P. Compression behavior of nanocrystalline anatase TiO_2, *Solid State Comm.*, 125, 111-115, 2003
60. Tarasov, B. P., Maehlen, J. P., Lototsky, M. V., Muradyan, V. E., Yartys, V. A. Hydrogen sorption properties of arc generated single-wall carbon nanotubes, *J. of Alloys & Compounds*, 356-357, 510-514, 2003
61. Thorkildsen, G., Larsen, H.B., Weckert, E., Semmingsen, D. Three-beam X-ray diffraction - Profile analysis, *J. of Appl. Cryst.*, 36, 1324-1333, 2003
62. Woodward, P.M., Karen, P. Mixed Valence in $YBaFe_2O_5$, *Inorganic Chem*., 42, 1121-1129, 2003
63. Woodward, P.M., Suard, E., Karen, P. Structural tuning of charge, orbital, and spin ordering in double-cell perovskite series between $NdBaFe_2O_5$ and $HoBaFe_2O_5$, *J. Am. Chem. Soc*. 125, 8889-8899, 2003
64. Yartys, V.A., De Boer, F.R., Buschow, K.H.J., Ouladdiaf, B., Brinks, H.W., Hauback, B.C. Crystallographic and magnetic structure of $Pr_6Fe_{13}AuD_{13}$, *J. of Alloys & Compounds*, 356-357, 142-146, 2003
65. Yartys, V.A., Isnard, O., Riabov, A.B., Akselrud, L.G. Unusual effects on hydrogenation: anomalous expansion and volume contraction, *J. of Alloys & Compounds*, 356-357, 109-113, 2003
66. Yartys, V.A., Ouladdiaf, B., Isnard, O., Khyzhum, O.Yu, Buschow, K.H.J. Hydrogen induced antiferromagnetism in the Kondo semimetal CeNiSn, *J. of Alloys & Compounds*, 359, 62-65, 2003

2004

1. Ammar, A., Ménétrier, M., Villesuzanne, A., Matar, S., Chevalier, B., Etourneau, J. Investigation of the electronic and structural properties of potassium hexaboride, KB_6, by transport, magnetic susceptibility, EPR, and NMR measurements, temperature-dependent crystal structure determination, and electronic band structure calculations, *Inorg. Chem.*, 43 (16), 4974 - 4987, 2004
2. Atkinson, T., Fjellvag, H., Kjekshus, A. Sinthesis, structure, and properties of chromium (111) sulfates, *J.Solid State Chem*., 177, 4351-4358, 2004
3. Bäerlocher, C., McCusker, L.B., Prokic, S., Wessels, T. Exploiting texture to estimate the relative intensities of overlapping reflections, *Z.Kristallogr*., 219, 803-812, 2004
4. Belyakova, O. A., Zubavichus, Y. V., Neretin, I. S., Golub, A. S., Novikov, Yu. N., Mednikov, E. G., Vargaftik, M. N., Moiseev, I. I., Slovokhotov, Yu. L. Atomic structure of nanomaterials: combined X-ray diffraction and EXAFS studies, *J. of Alloys & Compounds*, 382, 46-53, 2004
5. Birkedal, H., Madsen, D., Rangvald, H.M., Knudsen, K., Weber, H-P., Pattison, P., Schwarzenbach, D. The charge density of urea from synchrotron diffraction data, *Acta Cryst*. A60, 371-381, 2004
6. Bjørk, A., Dalhus, B., Mantzilas, D., Sirevåg, R., Eijsink, V. G.H. Large improvement in the thermal stability of a tetrameric malate dehydrogenase by single point mutations at the dimer–dimer interface, *J. of Mol. Biol*., 341, 1215-1226, 2004
7. Blanchard, D., Brinks, H.W., Hauback, B.C., Norby, P. Desorption of $LiAlH_4$ with Ti-and V-based additives, *Material Science & Engineering*, B108, 54-59, 2004
8. Boldyreva, E.V. High-pressure studies of the hydrogen bond networks in molecular crystals, *J. Mol. Structure*, 700, 151-155, 2004
9. Boldyreva, E., Drebushchak, T., Shakhtshneider, T., Sowa, H., Ahsbahs, H., Goryainov, S., Ivashevskaya, S., Kolesnik, E., Drebushchak, V., Burgina, E. Variable-temperature and variable-pressure studies of small-molecule organic crystals, *ARKIVOC*, xii, 128-155, 2004
10. Boldyreva, E.V., Ivashevskaya, S.N., Sowa, H., Ashbahs, H., Weber, H.-P. Effect of high pressure on crystalline glycine: A new high-pressure polymorph, *Doklady Physical Chemistry*, 396, 111-114, 2004
11. Brinks, H.W., Jensen, C.M., Srinivasan, S.S., Hauback, B.C., Blanchard, D., Murphy, K. Synchrotron X-ray and neutron diffraction studies of $NaAlH_4$ containing Ni additives, *J. of Alloys & Compounds*, 376, 215-221, 2004
12. Brodski, V., Peschar, R., Schenk, H., Brinkmann, A., Van Eck, E.R.H., Kentgens, A.P.M., Coussens, B. et al. Structure of melaminium dihydrogenpyrophospate and its formation from melaminium dihydrogenphosphate studied with powder diffraction data, solid-state NMR, and theoretical calculations, *J.Phys.Chem. B*, 108, 15069-15076, 2004

13. Cerny, R., Renaudin, G., Favre-Nicolin, V., Hlukhyy, V., Poettgen, R. $Mg_{1+x}Ir_{1-x}$(x=0, 0.037 and 0.054), a binary intermetallic compound with a new orthorhombic structure type determined from powder and single-crystal X-ray diffraction, *Acta Cryst*., B60, 272-281, 2004

14. Coronado, E., Gimenez-Saiz, C., Gomez-Garcia, C.J., Capelli, S.C. Metallic conductivity down to 2K in a polyoxometalate-containing radical salt of BEDO-TTF, *Angew. Chem. Int*., 43, 3022-3025, 2004

15. Coronado, E., Galan-Mascaros, J.R., Gimenez-Saiz, C., Gomez-Garcia, C.J., Martinez-Ferrero, E., Almeida, M., Lopes, E.B. et al. New conducting radical salts based upon Keggin-type polyoxometalates and perylene, *Materials Chem*., 12, 1867-1872, 2004

16. De Ridder, D.J.A., Goubitz, K., Brodski, V., Peschar, R., Schenk, H. Crystal Structure of melaminium orthophosphate from high-resolution synchrotron powder-diffraction data, *Helvetica Chimica Acta*, 87, 1894-1905, 2004

17. Dmitriev V., Kuznetsov A., Bandilet O., Bouvier P., Dubrovinsky L., Machon D., Weber H.-P. Stability of high-pressure monoclinic in Ce and Pr metals: Comparative diffraction study and phenomenological theory *Phys.Rev.*, B70, 014104, 2004

18. Dova, E., Peschar, R., Sakata, M., Kato, K., Stassen, A.F., Schenk, H. Haasnoot, J.G. Structures of FeII spin-crossover complexes from synchrotron powder-diffraction data, *Acta Cryst.* B60, 528-538, 2004

19. Dubrovinsky, L., Dubrovinskaia, N., Langenhorst, F., Dobson, D., Rubie, D., Geßmann, C., Le Bihan, T., Crichton, W. A. Reaction of iron and silica at core–mantle boundary conditions, *Phys. Earth and Planetary. Interiors*, 146, 243-247, 2004

20. Dubrovinsky, L., Dubrovinskaia, N., Prakapenka, V., Seifert, F., Langenhorst, F., Dmitriev, V., Weber, H.-P., Le Bihan, T. A class of new high-pressure silica polymorphs, *J.Phys. Earth and Planetary Interiors*, 143-144, 231-240, 2004

21. Ferbitz, L., Maier, T., Patzelt, H., Bukau, B., Deuerling, E., Ban, N. Trigger factor in complex with the ribosome forms a molecular cradle for nascent proteins, *Nature*, 431, 590 - 596, 2004

22. Filinchuk, Y.E., Birkedal, H., Cerny, R., Hostettler, M., Yanson, T.I., Bodak, O.I., Yvon, K. Chemical heterogeneity of a crystal built of nanoscale coherently twinned $Yb_{2-x}(Fe,Ga)_{17+2x}$ Polytypes, *Chem. Eur. J*., 10, 2972-2976, 2004

23. Fossdal, A., Brinks, H. W., Fichtner, M., Hauback, B.C. Determination of the crystal structure of $Mg(AlH_4)_2$ by combined X-ray and neutron diffraction, *J. of Alloys & Compaunds*, 387, 47-51, 2005

24. Franz, P., Ambrus, C., Hauser, A., Chernyshov, D., Hostettler, M., Hauser, J., Keller, L. et al. Crystalline, mixed-valence manganese analogue of prussian blue: magnetic, spectroscopic, x-ray and neutron diffraction studies *J. Am. Chem. Soc.*, 126, 16472-16477, 2004

25. Gardiner, C.H., Boothroyd, A.T., Pattison, P., McKelvy, M.J., McIntyre, G.J., Lister, S.J.S. Cooperative Jahn-Teller distortion in PrO_2, *Phys. Rev*., B70, 24415, 2004

26. Grebille. D., Lambert, S., Bouree, F., Petricek, V. Contribution of powder diffraction for structure refinements of aperiodic misfit cobalt oxides, *J. Appl. Crystallogr.*, 37, 823-831, 2004

27. Grunwaldt, J-D., Caravati, M., Hannemann, S., Baiker, A. X-ray absorption specroscopy under reaction conditions: suitability of different reaction cells for combined catalyst characterization and time-resolved studies, *Phys. Chem. Chem. Phys*., 6, 3037-3047, 2004

28. Grzechnik, A., Dmitriev, V., Weber, H-P., Gesland, J-Y., Van Smaalen, S. The crystal structures of pressure-induced $LiSrAlF_6$-II and $LiCaAlF_6$-II, *J. Phys.: Condens. Matter*, 16, 1033-1043, 2004

29. Grzechnik A., Dmitriev V., Weber H.-P., Gesland J.-Y., Friese K. Anisotropic thermal expansion in $LiCaAlF_6$ and $LiSrAlF_6$, *J.Phys.: Condens. Matter*, 16, 5769, 2004

30. Grzechnik, A., Dmitriev, V., Weber, H-P., Gesland, J-Y., Van Smaalen, S. $LiSrAlF_6$ with $LiBaCrF_6$-type structure, *J.Phys.: Condens. Matter*, 16, 3005-3013, 2004

31. Grzechnik A., Crichton W., Bouvier P., Dmitriev V., Weber H.-P., Gesland J.-Y. Decomposition of $LiGdF_4$ scheelite at high pressures, *J.Phys.: Condens. Matter*, 16, 7779-7786, 2004

32. Hansteen, O.H., Bréard, Y., Fjellvag, H., Hauback, B.C. Divalent manganese in reduced $LaMnO_{3-}$ - effect of oxygen nonstoichiometry on structural and magnetic properties, *Solid State Sciences*, 6, 279-285, 2004

33. Hostettler, M., Töernroos, K.W., Chernyshov, D., Vangdal, B., Büergi, H-B. Challenges in engineering spin crossover: structures and magnetic properties of six alcohol solvates of Iron (II) Tris(2-picolylamine) Dichloride, *Angew. Chem. Int.*, 43, 4589-4594, 2004

34. Hostettler, M., Schwarzenbach, D., Helbing, J., Dmitriev, V., Weber, H-P. Structure and SHG of

the high pressure phase IV of $HgBr_2$, *Solid State Comm*., 129, 359-363, 2004

35. Karen, P. Chemistry and thermodynamics of the twin charge-ordering transitions in $RBaFe_2O_{5+w}$ series, *J. of Solid State Chem*., 177, 281-292, 2004

36. Karppinen, M., Fjellvag, H., Konno, T., Morita, Y., Motohashi, T., Yamauchi, H. Evidence for oxygen vacancies in misfit-layered calcium cobalt oxide $[CoCa_2O_3]qCoO_2$, *Chem. Mater*., 16, 2790-2793, 2004

37. Kobas, M., Weber, Th., Seurer, W. Modelling disorder of decagonal Al-Co-Ni quasicrystals, *Ferroelectrics*, 305, 185-188, 2004

38. Kolberg, M., Strand, K.R., Graff, P., Andersson, K.K. Structure, function, and mechanism of ribonucleotide reductases, *Biochim. et Biophys. Acta*, 1699, 1-34, 2004

39. Krauss, G., Steurer, W. A single-crystal high-pressure x-ray diffraction study of decagonal Al-Co-Cu up to 19.1 GPa, *J. Phys.: Condens. Matter*, 16, 7769-7777, 2004

40. Krivovichev, S.V., Yakovenchuck, V.N., Armsbruster, T., Doebelin, N., Pattison, P., Weber, H.-P., Depmeier, W. Porous titatonisilicate nanorods in the structure of yuksporite, $(Sr,Ba)_2K_4(Ca,Na)_{14}(Mn,Fe)\{(Ti,Nb)_4(O,OH)_4[Si_6O_{17}]_2[Si_2O_7]_3\}(H_2O,OH)_n$, resolved using synchrotron radiation, *American Mineralogist*, 89, 1561-1565, 2004

41. Krivovichev, S.V., Yakovenchuck, V.N., Armsbruster, T., Pakhomovsky, Y. A., Weber, H.-P., Depmeier, W. Synchrotron X-ray diffraction study of the structure of shafranovskite, $K_2Na_3(Mn,Fe,Na)_4[Si_9(O,OH)_{27}](OH)_2\ H_2O$, a rare manganese phyllosilicate from the Kola peninsula, Russia, *American Mineralogist*, 89, 1816-1821, 2004

42. Leiros, I., McSweeney, S., Hough, E. The reaction mechanism of phospholipase D from streptomyces sp. Strain PMF. Snapshots along the reaction pathway reveal a pentacoordinate reaction intermediate and an unexpected final product, *J. Mol. Biol*., 339, 805-820, 2004

43. Machon, D., Dmitriev, V., Sinitsyn, V., Lucazeau, G. $Eu_2(MoO_4)_3$ single crystal at high pressure: Structural phase transition and amorphization probed by fluorescence spectroscopy, *Phys.Rev.*, B70, 094117, 2004

44. Mattesini, M., Almeida, S., Dubrovinsky, L., Dubrovinskaia, N., Johansson, B., Ahuja, R. High-pressure and high-temperature synthesis of the cubic TiO_2 polymorph, *Phys. Rev*., B70, 212101, 2004

45. Millini, R., Carluccio, L., Carati, A., Bellussi, G., Perego, C., Cruciani, G., Zanaddi, S. ESR-12 A new layered tetramethylammonium silicate composed by ferrierite layers, *Microp. & Mesop. Materials*, 74, 59-71, 2004

46. Moe, E., Leiros, I., Riise, E. K., Olufsen, M., Lanes, O., Smalås, A. O., Willassen, N. P. Optimisation of the surface electrostatics as a strategy for cold adaptation of uracil-DNA N-glycosylase (UNG) from atlantic cod (Gadus morhua), *J. Mol. Biol*., 343, 1221-1230, 2004

47. Nilsson, K., Hersleth, H-P., Rod, T. H., Andersson, K.K., Ryde, U. The protonation status of compound II in myoglobin, studied by a combination of experimental data and quantum chemical calculations: quantum refinement, *Biophys. Journal*, 87, 3437-3447, 2004

48. Pan, Y., Birkedal, H., Pattison, P., Brown, D., Chapuis, G. Molecular dynamics study of triptophylglycine: a dipeptide nanotube with confined water, *J. Phys. Chem. B,* 108,6458-6466, 2004

49. Peschar, R., Pop, M.M., De Ridder, D.J.A., Van Mechelen, J.B., Driessen, R.A.J., Schenk, H. Crystal structures of 1,3-Distearoyl-2-oleoylglycerol and cocoa butter in the beta(V) phase reveal the driving force behind the occurrence of fat bloom on chocolate, *J. Phys. Chem. B*, 108, 15450-15453, 2004

50. Pirngruber, G. D., Luechingera, M., Roy, P. K., Cecchetto, A., Smirniotis, P. N_2O decomposition over iron-containing zeolites prepared by different methods: a comparison of the reaction mechanism, *J. of Catalysis*, 224, 429-440, 2004

51. Pirngruber, G. D., Roy, P. K., Weiher, N. An in Situ X-ray absorption spectroscopy study of N_2O decomposition over Fe-ZSM-5 prepared by chemical vapor deposition of $FeCl_3$, *J. Phys. Chem. B,* 108, 13746 -13754, 2004

52. Przenioslo, R., Sosnowska, I., Van Beek, W., Suard, E., Hewat, A. Phase separation in $CaCu_xMn_{7-x}O_{12}(x=0.38)$, *J. of Alloys & Compounds*, 362, 218-223, 2004

53. Ramstad, A. L., Mikkelsen, Ø. Structural characterisation of copper-containing manganese oxide octahedral molecular sieve (Cu-OMS-2) materials by X-ray absorption spectroscopy and cyclic voltammetry, *J. of Mol. Structure*, 697, 109-117, 2004

54. Rukiah, M., Lefebvre, J., Hernander, O., Van Beek, W., Serpelloni, M. Ab initio structure determination of the Gamma-form of D-sorbitol (D-glucitol) by powder synchrotron X-ray diffraction, *J. Appl. Crystallogr.*, 37, 766-772, 2004

55. Schenk, H., Peschar, R. Understanding the structure of chocolate, *Radiation Phys. and Chem*., 71, 829-835, 2004
56. Schoenleber, A., Chapuis, G. Quininium (R)-mandelate, a structure with large Z' described as an incommensurately modulated structure in (3+1)-dimensional superspace, *Acta Cryst*., B60, 108-120, 2004
57. Schrøder Leiros, H.-K., Brandsdal, B. O., Andersen, O. A., Os, V., Leiros, I., Helland, R., Otlewski, J., Willassen, N. P., Smalås, A. O. Trypsin specificity as elucidated by LIE calculations, X-ray structures, and association constant measurements, *Protein Science*, 13, 1056-1070, 2004
58. Simoncic, P., Armbruster, T. Peculiarity and defect structure of the natural and synthetic zeolite mordenite: A single-crystal X-ray study, *American Mineralogist*, 89, 421-431, 2004
59. Simoncic, P., Armbruster, T. Se incorporated into zeolite mordenite-Na: a single crystal x-ray study, *Microporous & mesoporous Materials*, 71, 185-198, 2004
60. Simoncic, P., Armbruster, T., Pattison P. Cationic Thionin Blue in the Channels of Zeolite Mordenite: A Single-Crystal X-ray Study, *J. Phys. Chem. B*, 108, 17352-17360, 2004
61. Sinitsyn, V., Dmitriev, V., Bdikin, I., Machon, D., Dubrovinsky, L., Ponyatovsky, E., Weber, H.-P. Amorphization of cuprite, Cu_2O, due to chemical decomposition under high pressure, *JETP Letters*, 80, 831-834, 2004
62. Srinivasan, S.S., Brinks, H.W., Hauback, B.C., Sun, D., Jensen, C.M. Long term cycling behavior of titanium doped $NaAlH_4$ prepared through solvent mediated milling of NaH and Al with titanium dopant precursors, *J. of Alloys and Compounds*, 377, 283-289, 2004
63. Stel'makh, S., Gierlotka, S., Grzanka, E., Weber, H. -P., Palosz, B. X-ray diffraction studies of thermal properties of the core and surface shell of isolated and sintered SiC nanocrystals, *J. of Alloys and Compounds*, 382, 138-145, 2004
64. Steurer, W. Twenty years of structure research on quasicrystals. Part I. Pentagonal, octagonal, decagonal and dodecagonal quasicrystals, *Z. Kristallogr.*, 219, 391-446, 2004
65. Steurer, W. *Present state of knowledge on quasicrystals* in "Applied Crystallography: Proc. of the XIX Conference, Krakow, Poland, 1 - 4 September 2003" , eds. Morawiec, H., Stroz, D., (World Scientific Publ. Comp., 2004), 254
66. Krauss, G., Steurer, W. *Why study quasicrystals at high pressures?* in "High-Pressure Crystallography", eds. Katrusiak, A., McMillan, P. F., (Kluwer, 2004), 521 T
67. Strand, K.R., Karlsen, S., Kolberg, M., Rohr, A.K., Goerbitz, C.H., Andersson, K.K. Crystal structure studies of changes in the native dinuclear iron center of ribonucleotide reductase protein R2 from mouse, *J.Biol.Chem*., 279, 46794-46801, 2004
68. Struis, R.P.W.J., Ludwig, C., Lutz, H., Scheidegger, A.M. Speciation of Zinc in municipal solid waste incineration fly ash after heat treatment: an x-ray absorption spectroscopy study, *Environ. Sci. Technol.*, 38, 3760-3767, 2004
69. Weber, Th., Kobas, M., Steurer, W. The disordered 8 Å superstructure of a decagonal $Al70Co_{12}Ni_{18}$ quasicrystal, *Ferroelectrics*, 305, 213-216, 2004
70. Weitz-Schmidt, G., Welzenbach, K., Dawsen, J., Kallen, J. Improved lymphocyte function-associated antigen (LFA-1)-1 inhibition by statin derivatives, *J. Biol. Chem.*, 279, 46764-46771, 2004
71. Zanardi, S., Alberti, A., Cruciani, G., Corma, A., Fornes, V., Brunelli, M. Crystal structure determination of zeolite Nu-6(2) and its layered precursor Nu-6(1), *Angew. Chem. Int.*, 43, 4933-4937, 2004.